Three Modes of Crack Propagation

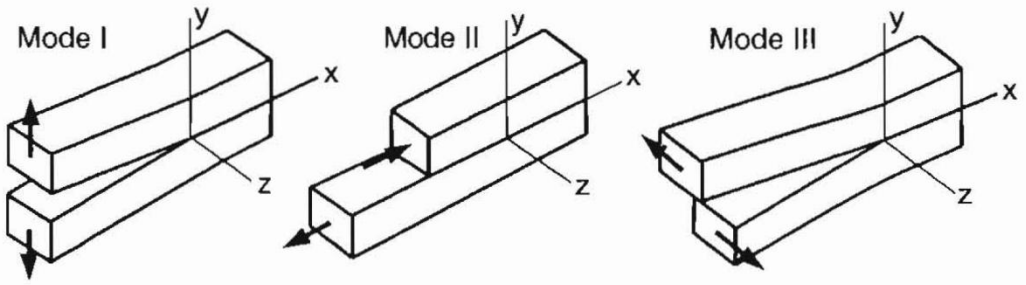

Figure 8.8 The basic modes of crack surface displacement. (Adapted from [Tada 85]; used with permission.)

From Mechanical Behavior
of Materials, Norman E. Dowling

Table 7.2 | Plane-Strain Fracture Toughnesses for Representative Materials

	Material	K_{Ic} (MPa $m^{1/2}$)
(a)	*Metals*	
	300M steel 300 °C temper	65
	300M steel 650 °C temper	152
	18-Ni maraging steel, vacuum melted	176
	18-Ni maraging steel, air melted	123
	AISI 4130 steel	110
	2024-T651 aluminum	24
	2024-T351 aluminum	34
	6061-T651 aluminum	34
	7075-T651 aluminum	29
	Ti-6Al-4V, mill annealed	106–123
	Ti-6Al-4V, recrystallized, annealed	77–116
(b)	*Ceramics*	
	Cement/concrete	0.2
	Soda–lime glass	0.7–0.9
	MgO	3
	Al_2O_3	3–5
	Al_2O_3 + 15% ZrO_2	10
	SiC	3–4
	Si_3N_4	4–5
(c)	*Polymers*	
	Epoxy	0.3–0.6
	Polyethylene, high-density	2
	Polyethylene, low-density	1
	Polypropylene	3
	ABS	3–4
	Polycarbonate	1–2.6
	PVC	2.4
	PVC (rubber modified)	3.4
	PMMA	1.8

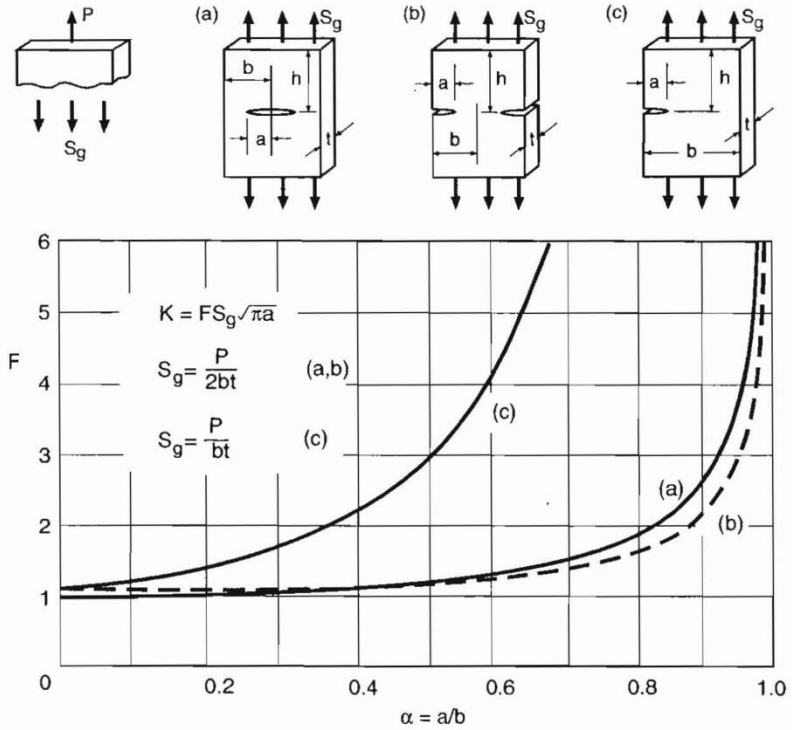

Values for small a/b and limits for 10% accuracy:

(a) $K = S_g\sqrt{\pi a}$ $(a/b \le 0.4)$ (b) $K = 1.12S_g\sqrt{\pi a}$ $(a/b \le 0.6)$ (c) $K = 1.12S_g\sqrt{\pi a}$ $(a/b \le 0.13)$

Expressions for any $\alpha = a/b$:

$$\text{(a)}\quad F = \frac{1 - 0.5\alpha + 0.326\alpha^2}{\sqrt{1-\alpha}} \qquad (h/b \ge 1.5)$$

$$\text{(b)}\quad F = \left(1 + 0.122\cos^4\frac{\pi\alpha}{2}\right)\sqrt{\frac{2}{\pi\alpha}\tan\frac{\pi\alpha}{2}} \qquad (h/b \ge 2)$$

$$\text{(c)}\quad F = 0.265\,(1-\alpha)^4 + \frac{0.857 + 0.265\alpha}{(1-\alpha)^{3/2}} \qquad (h/b \ge 1)$$

Figure 8.12 Stress intensity factors for three cases of cracked plates under tension. Geometries, curves, and equations labeled (a) all correspond to the same case, and similarly for (b) and (c). (Equations as collected by [Tada 85] pp. 2.2, 2.7, and 2.11.)

From Mechanical Behavior of Materials, Norman E. Dowling

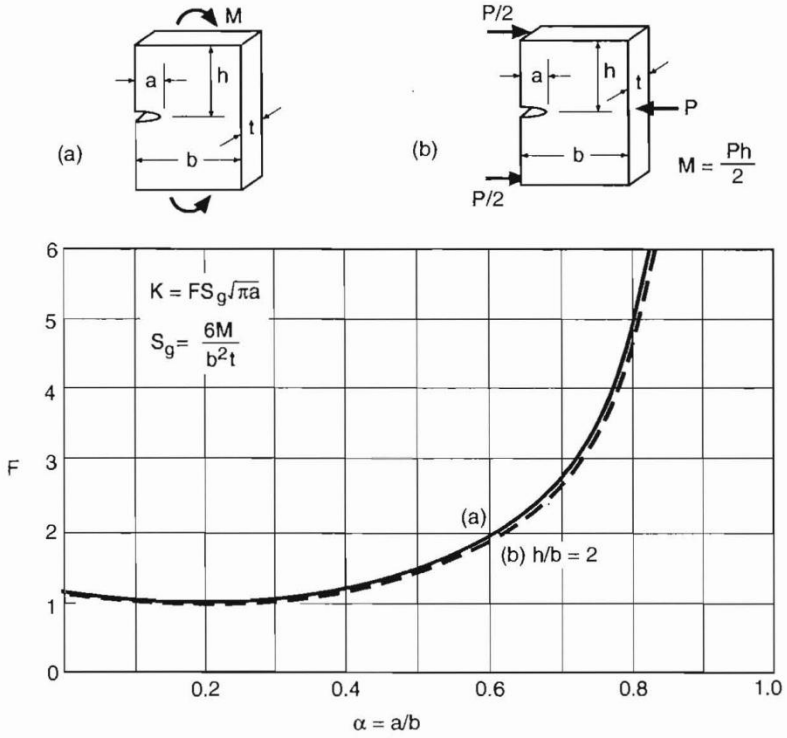

Values for small a/b and limits for 10% accuracy:

$$\text{(a, b)} \quad K = 1.12 S_g \sqrt{\pi a} \qquad (a/b \leq 0.4)$$

Expressions for any $\alpha = a/b$:

$$\text{(a)} \quad F = \sqrt{\frac{2}{\pi\alpha}\tan\frac{\pi\alpha}{2}}\left[\frac{0.923 + 0.199\left(1 - \sin\frac{\pi\alpha}{2}\right)^4}{\cos\frac{\pi\alpha}{2}}\right] \qquad \text{(large } h/b\text{)}$$

(b) F is within 3% of (a) for $h/b = 4$, and within 6% for $h/b = 2$, at any a/b:

$$F = \frac{1.99 - \alpha(1-\alpha)\left(2.15 - 3.93\alpha + 2.7\alpha^2\right)}{\sqrt{\pi}\,(1+2\alpha)\,(1-\alpha)^{3/2}} \qquad (h/b = 2)$$

Figure 8.13 Stress intensity factors for various cases of bending. Geometries, curves, and equations labeled (a) all correspond to the same case, and similarly for (b). Case (b) with $h/b = 2$ is the ASTM standard bend specimen. (Equations from [Tada 85] p. 2.14, and [ASTM 97] Std. E399.)

From Mechanical Behavior of Materials, Norman E. Dowling

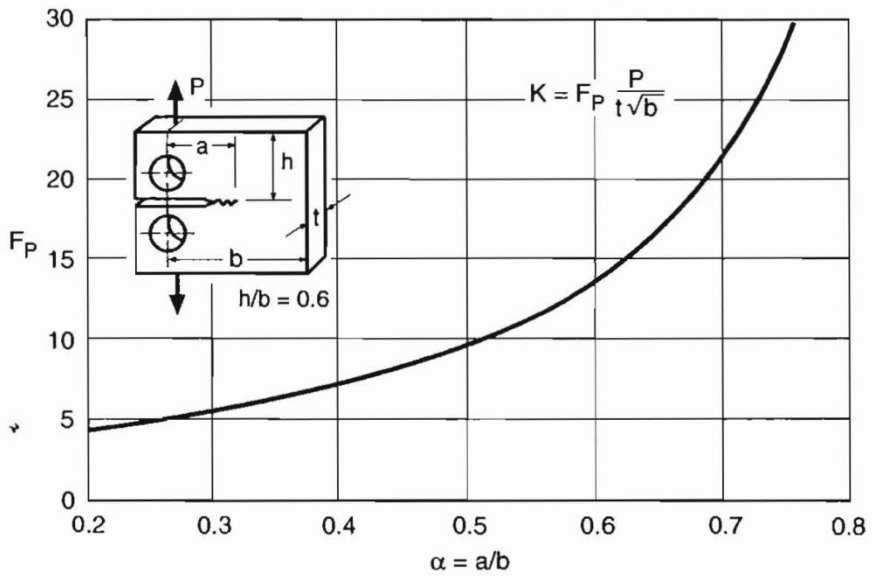

$$F_P = \frac{2+\alpha}{(1-\alpha)^{3/2}}(0.886 + 4.64\alpha - 13.32\alpha^2 + 14.72\alpha^3 - 5.6\alpha^4) \qquad (a/b \geq 0.2)$$

Figure 8.16 Stress intensity factor for the ASTM standard compact specimen, as determined from $F_P = F_P(\alpha)$, where $\alpha = a/b$. (Equation from [Srawley 76].)

From Mechanical Behavior of Materials, Norman E. Dowling

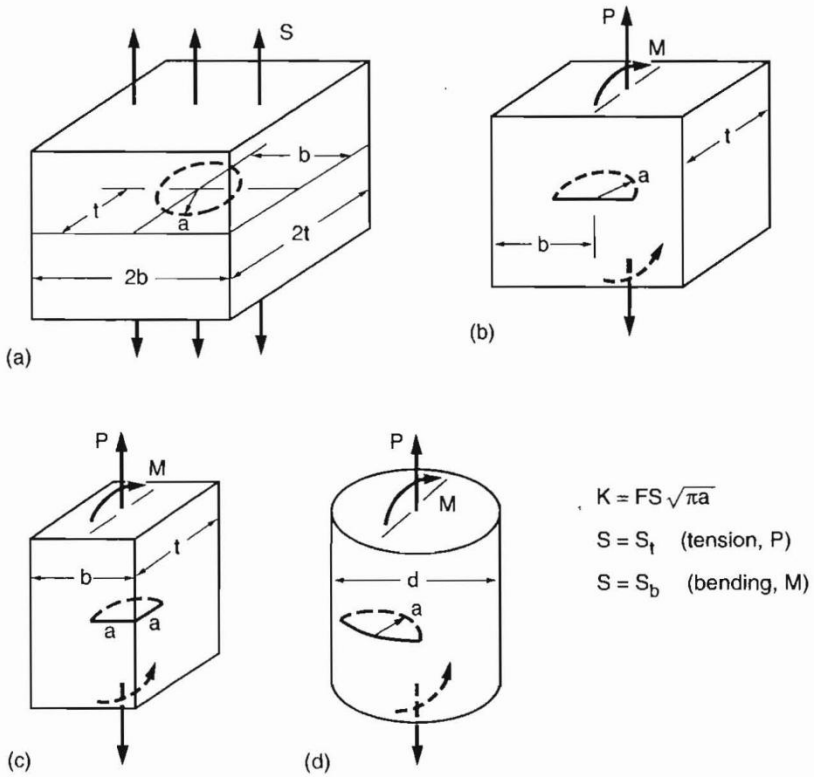

Case	S_t	S_b	F for small a	Limits for ±10% on F
(a)	$\frac{P}{4bt}$	—	$\frac{2}{\pi} = 0.637$	$\frac{a}{t}$, $\frac{a}{b} < 0.5$
(b)	$\frac{P}{2bt}$	$\frac{3M}{bt^2}$	0.728	$\frac{a}{t} < 0.4$, $\frac{a}{b} < 0.3$
(c)	$\frac{P}{bt}$	$\frac{6M}{bt^2}$	0.722	$\frac{a}{t} < 0.35$, $\frac{a}{b} < 0.2$
(d)	$\frac{4P}{\pi d^2}$	$\frac{32M}{\pi d^3}$	0.728	$\frac{a}{d} < 0.2$ or 0.35^1

Note: [1]Different limits for tension or bending, respectively.

Figure 8.17 Stress intensity factors for (a) an embedded circular crack under uniform tension normal to the crack plane, and related cases: (b) half-circular surface crack, (c) quarter-circular corner crack, and (d) half-circular surface crack in a shaft, where the latter is more precisely a portion of a circular arc with center on the surface. (Based on [Newman 86] and [Raju 86].)

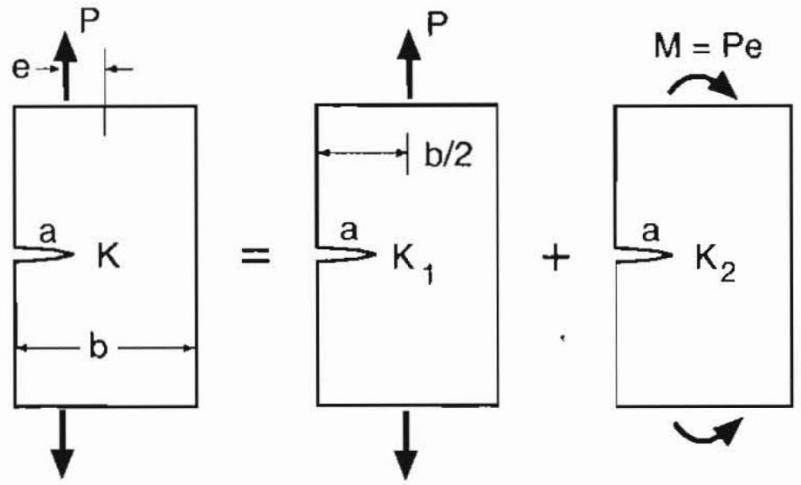

Figure 8.22 Eccentric loading of a plate with an edge crack, and the superposition used to obtain *K*.

From Mechanical Behavior
of Materials, Norman E. Dowling

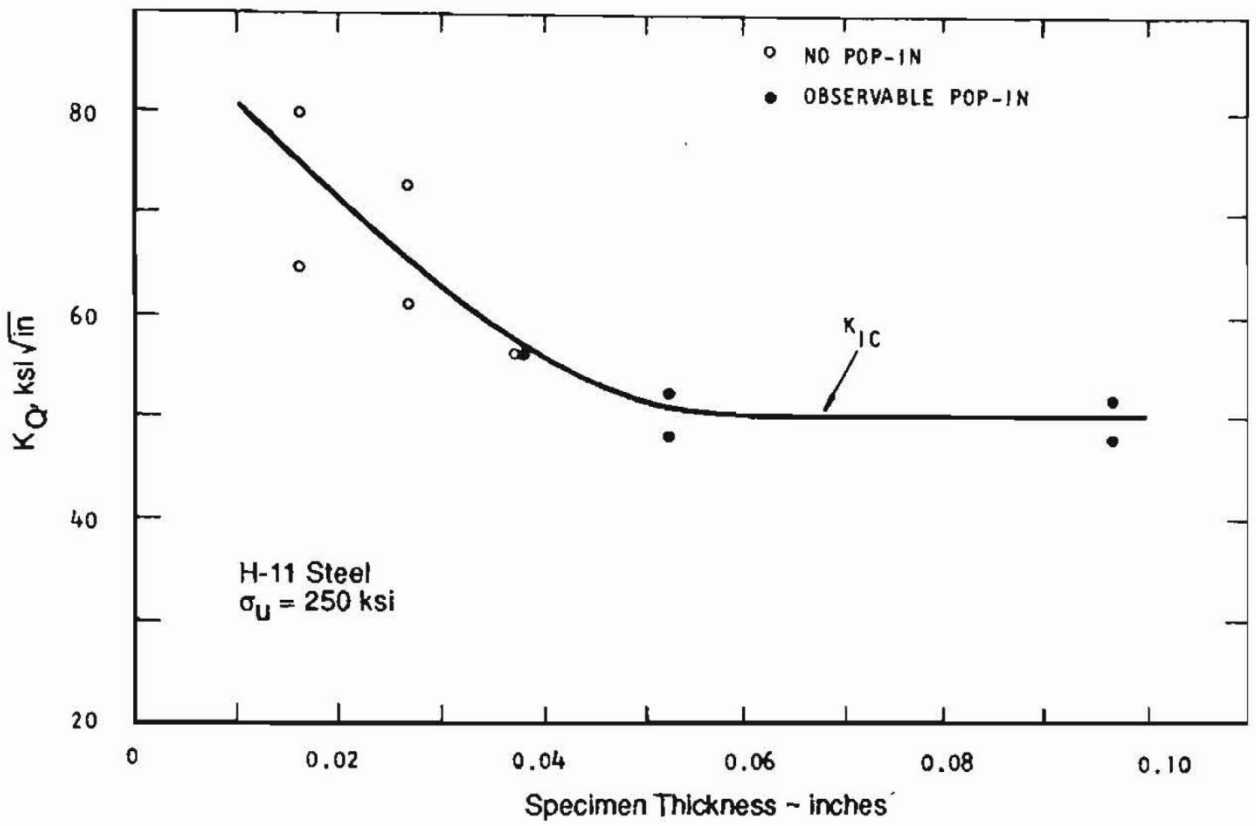

Figure 8.31 Effect of thickness on fracture toughness of an alloy steel heat treated to the high strength of $\sigma_u = 1720$ MPa. (Adapted from [Steigerwald 70]; copyright © ASTM; reprinted with permission.)

From Mechanical Behavior
of Materials, Norman E. Dowling

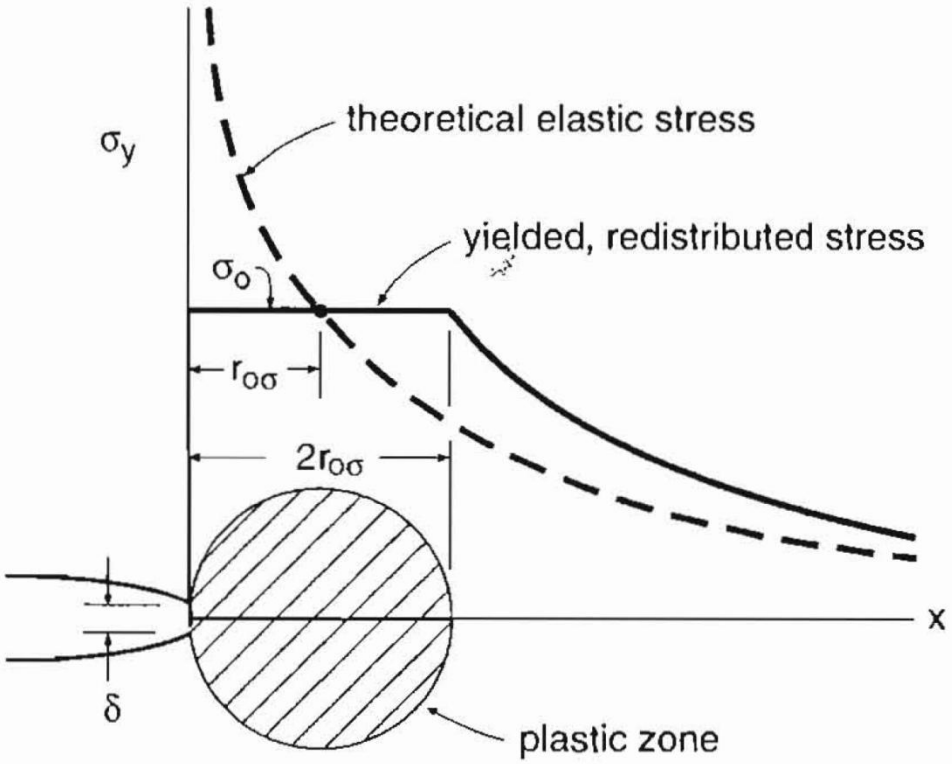

Figure 8.43 Plastic zone size estimate for plane stress, showing the approximate effect of redistribution of stress.

From Mechanical Behavior
of Materials, Norman E. Dowling

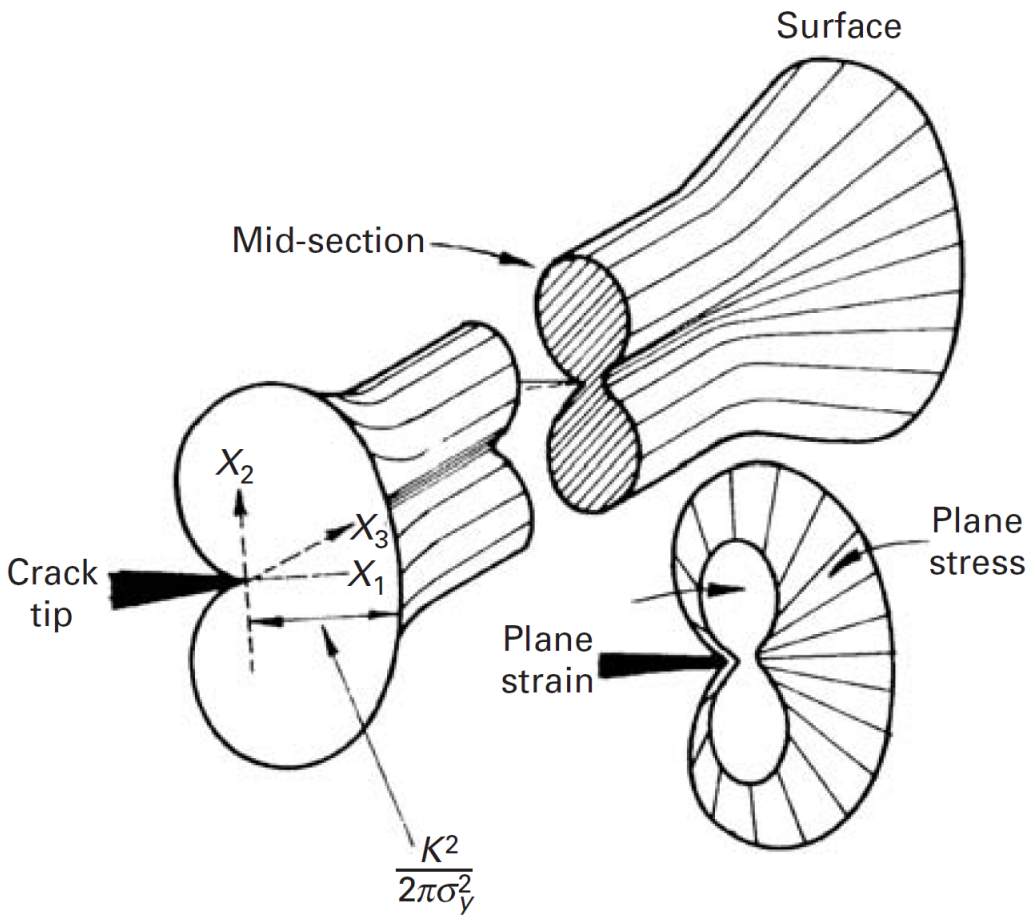

Fig. 7.16 Formal representation of the plastic zone at the crack tip for a through-the-thickness crack in a plate.

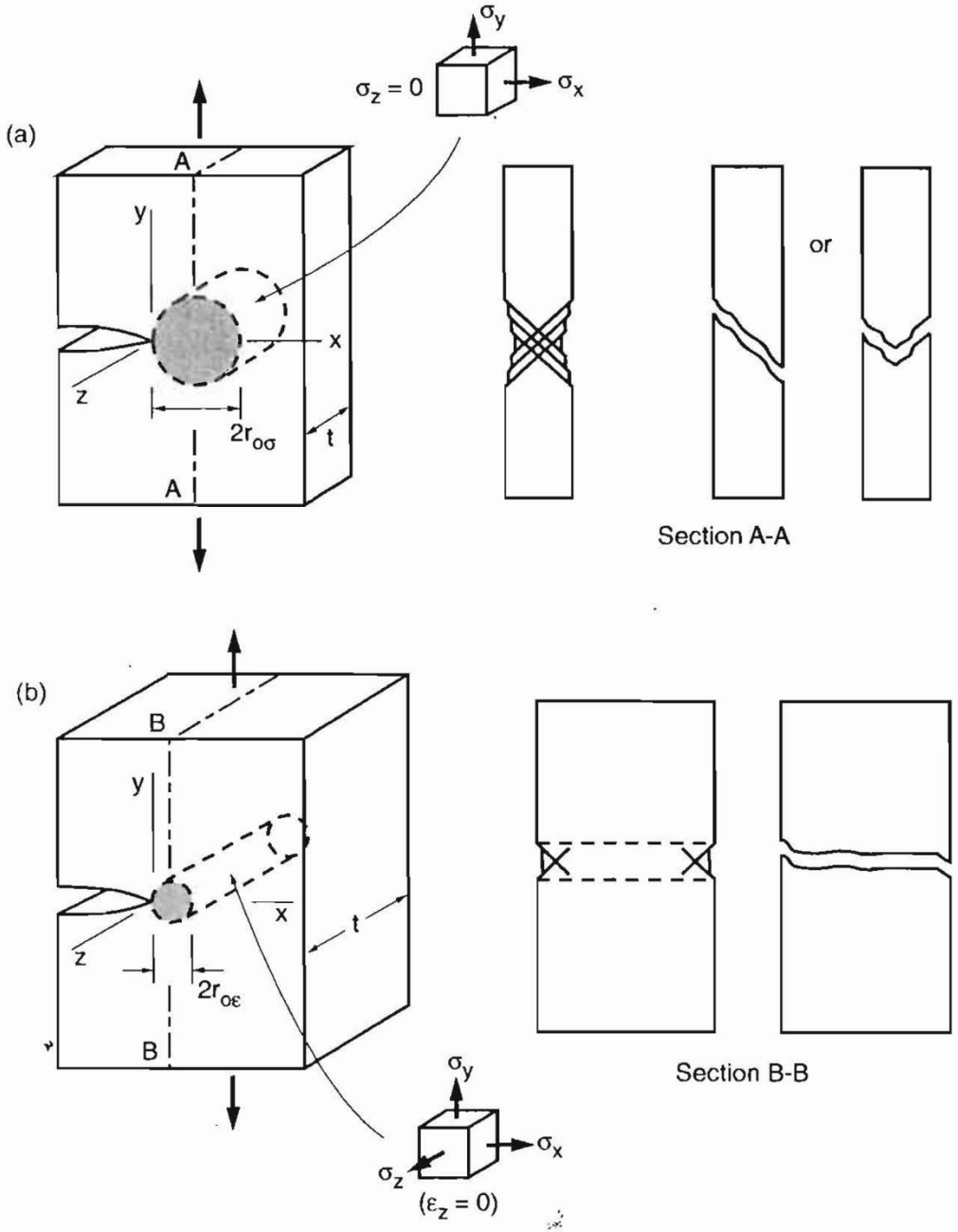

Figure 8.44 Plastic zone, stress state, and fracture mode for (a) plane stress and (b) plane strain.

From Mechanical Behavior of Materials, Norman E. Dowling

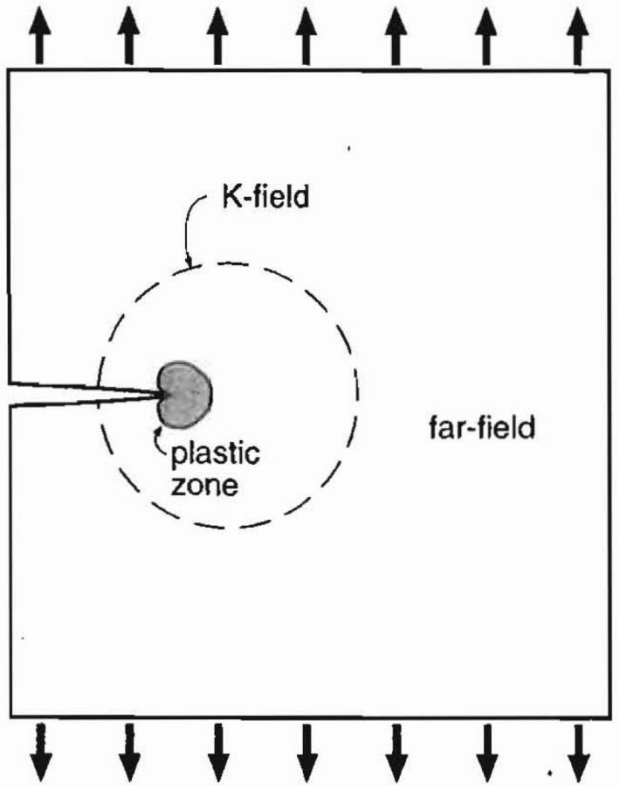

Figure 8.45 A crack and its plastic zone, and the larger *K*-field that must exist for LEFM to be applicable.

From Mechanical Behavior
of Materials, Norman E. Dowling

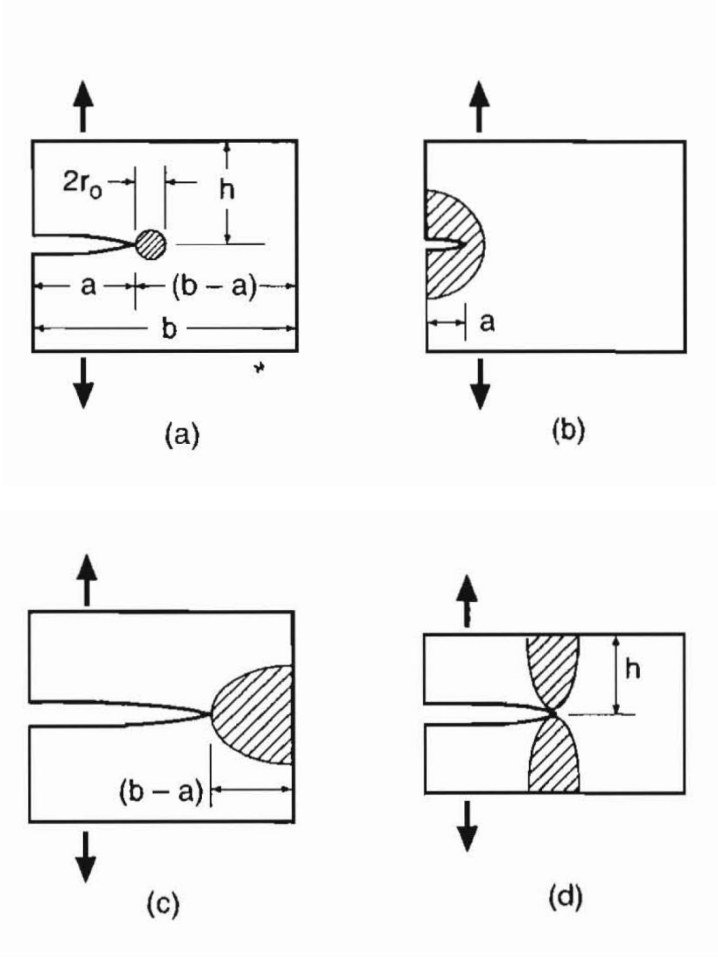

Figure 8.46 Small plastic zone compared with planar dimensions (a), and situations where LEFM is invalid due to the plastic zones being too large compared with (b) crack length, (c) uncracked ligament, and (d) member height.

From Mechanical Behavior of Materials, Norman E. Dowling

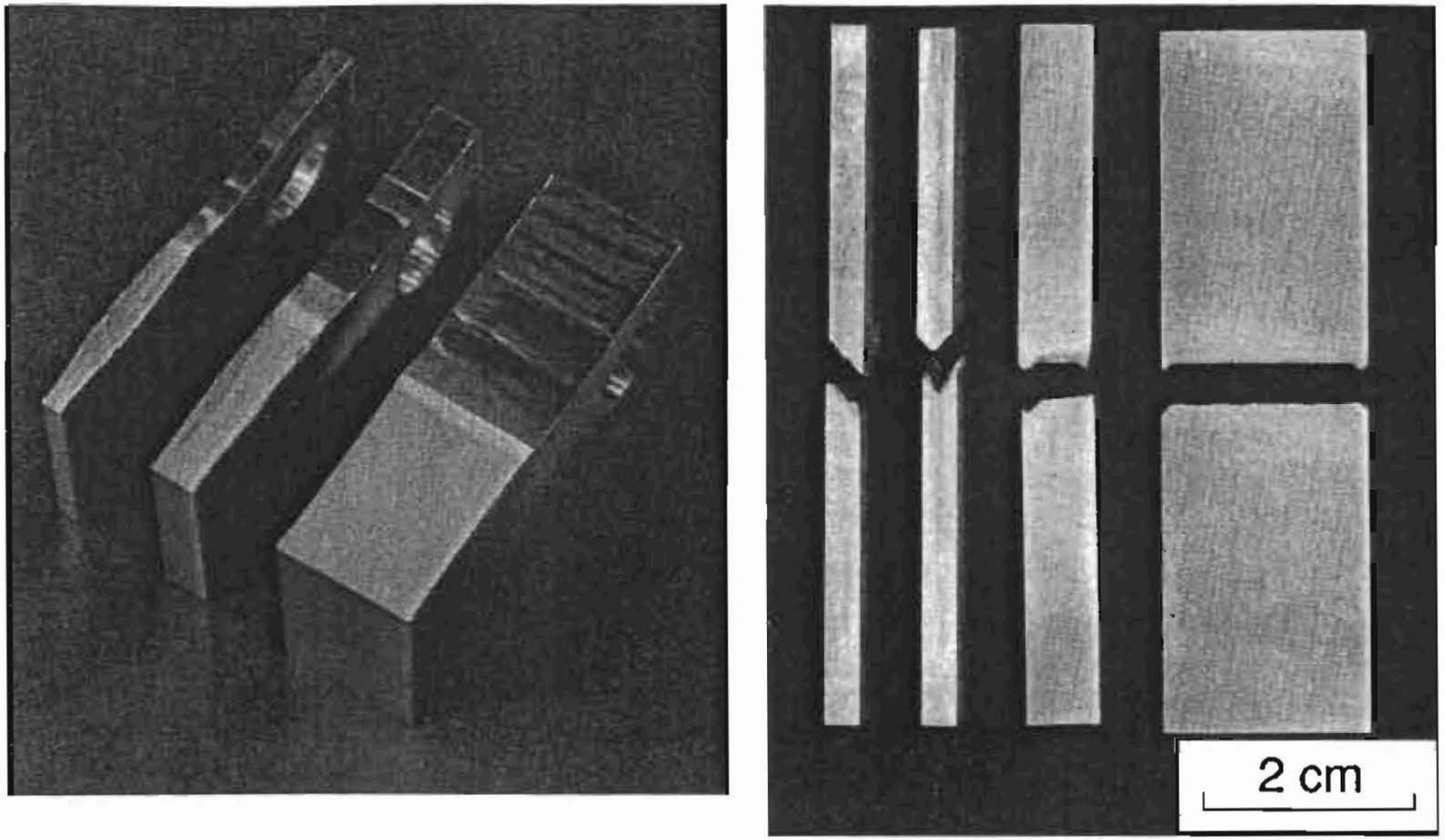

Figure 8.47 Fracture surfaces (left) and cross sections showing profiles of fractures (right) for toughness tests on compact specimens ($b = 51$ mm) of 7075-T651 aluminum. The thinnest specimens shown have typical plane stress fractures on inclined planes; the intermediate thickness has mixed behavior; and the thickest specimens have flat plane-strain fractures. (Photos by R. A. Simonds.)

From Mechanical Behavior of Materials, Norman E. Dowling

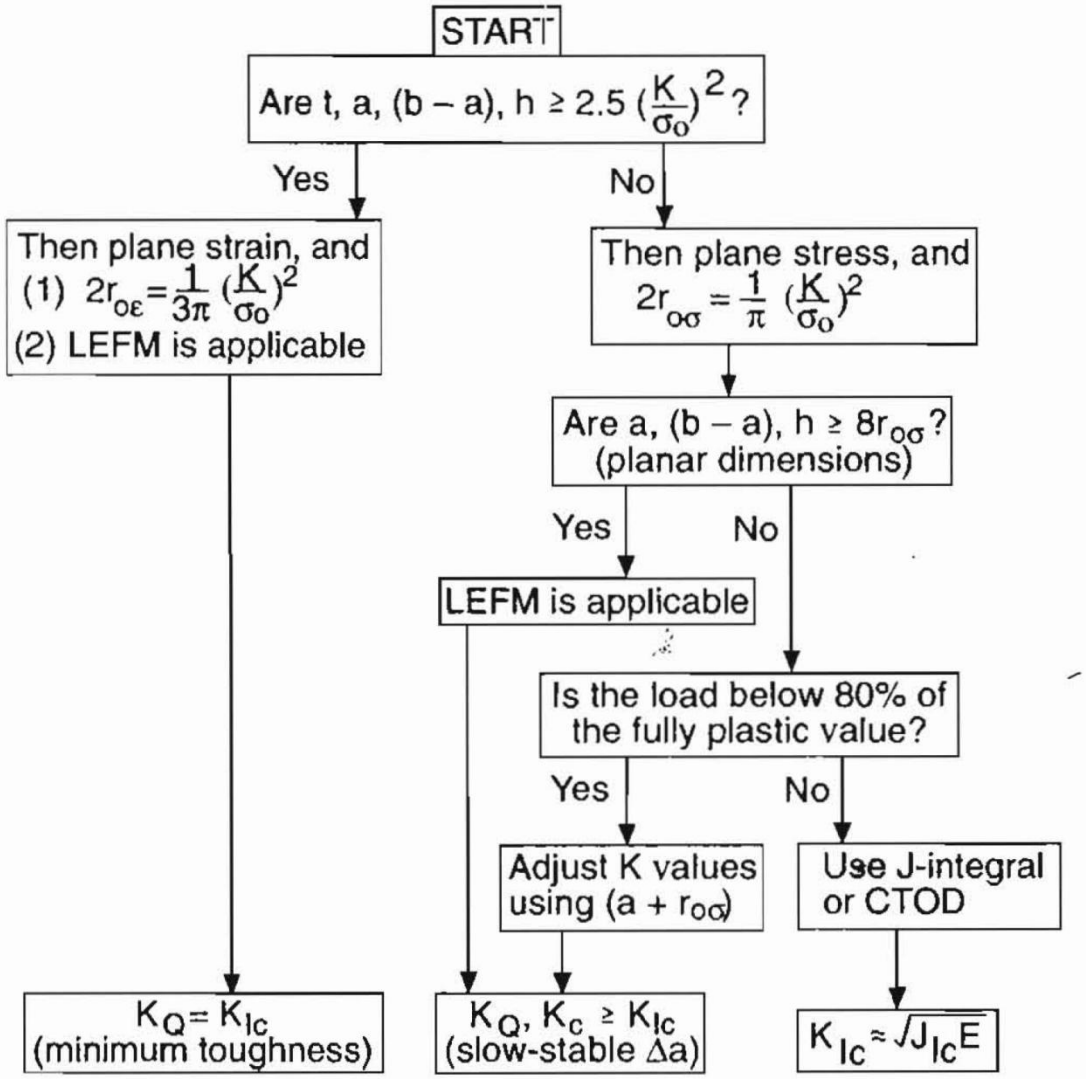

Figure 8.53 Flowchart for distinguishing between plane stress and plane strain, for deciding what fracture mechanics approach is needed, and for identifying what is expected from toughness testing.

From Mechanical Behavior of Materials, Norman E. Dowling

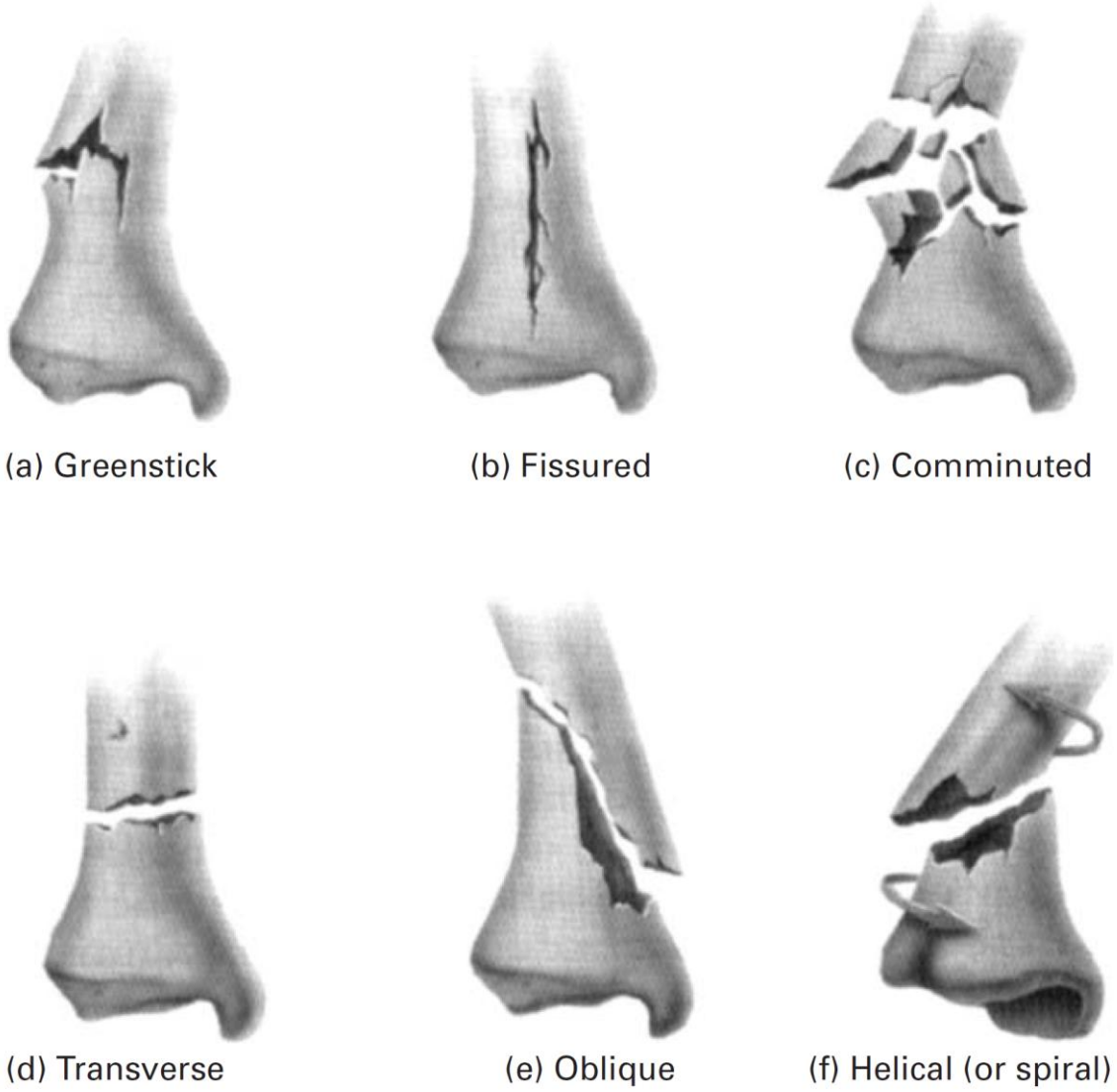

Six modes of fracture in bone. (Adapted from S. J. Hall, *Basic Biomechanics., 4th ed.* (Boston: McGraw Hill, 2003), p. 102.)

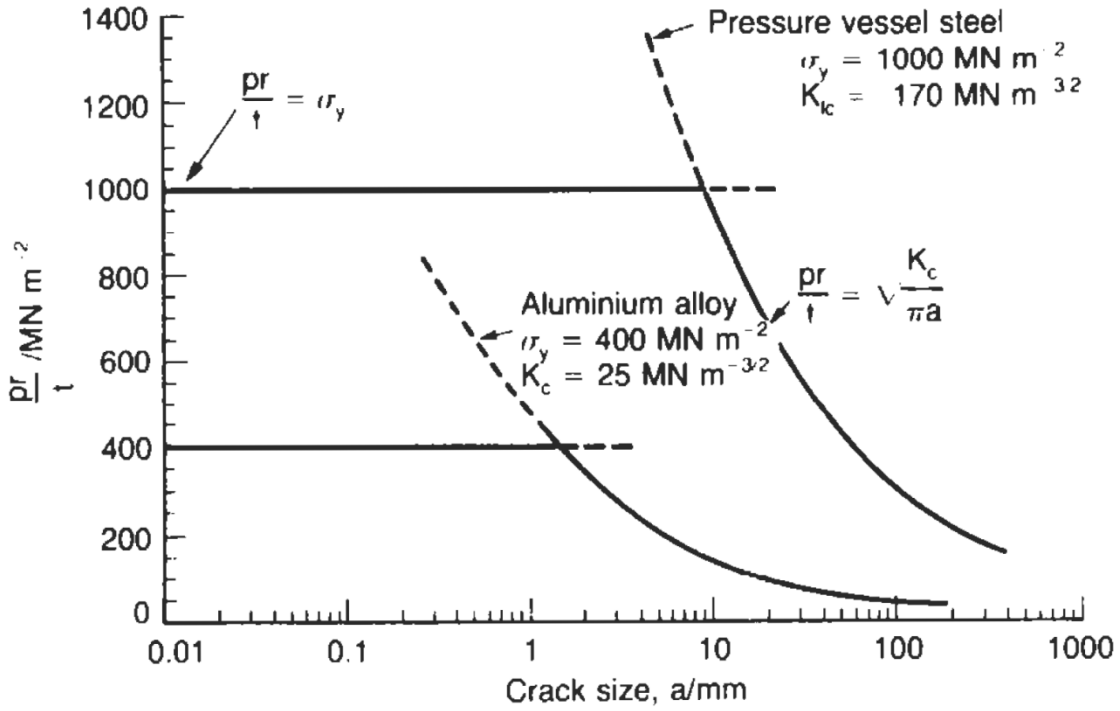

Fig. 16.6. Design against yield and fast fracture for a cylindrical pressure vessel.

Leak before Break: Design to Avoid Fast Fracture

Definitions

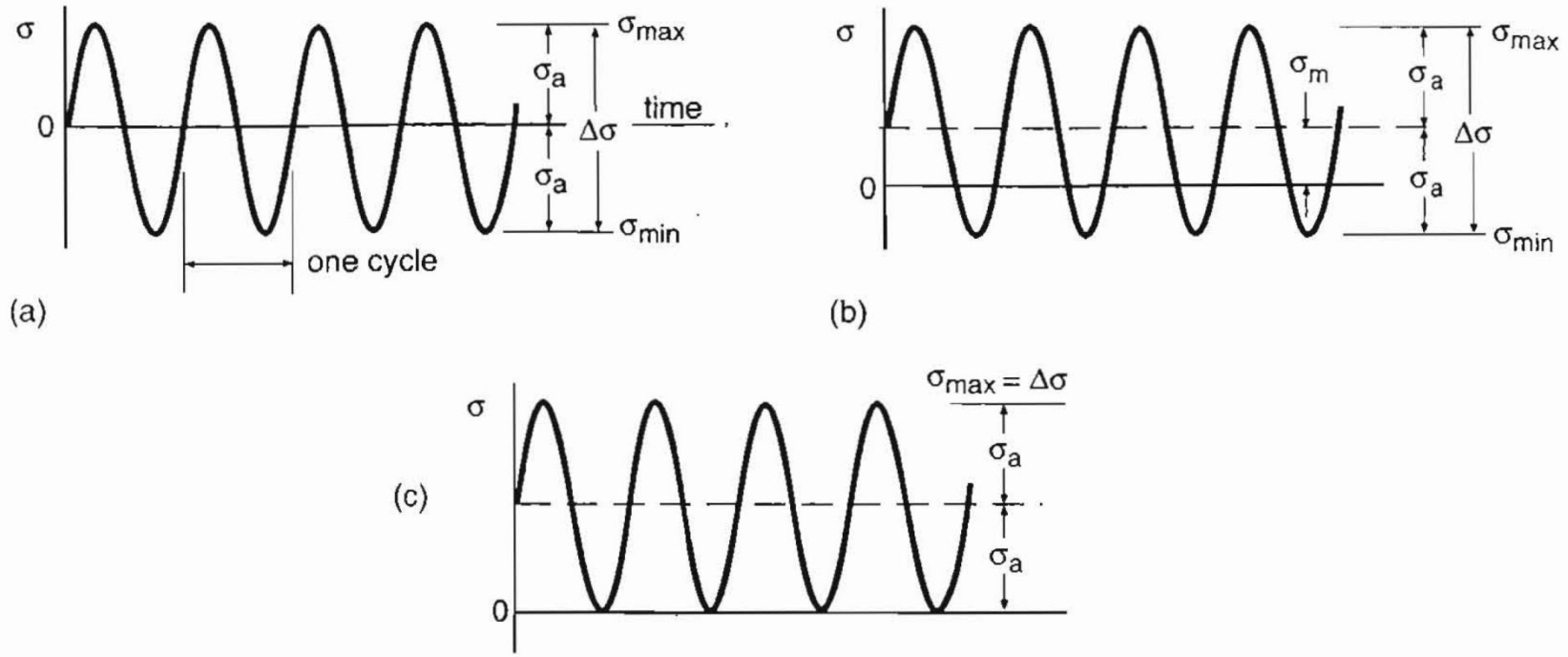

Figure 9.2 Constant amplitude cycling and the associated nomenclature. Case (a) is completely reversed stressing, $\sigma_m = 0$; (b) has a nonzero mean stress σ_m; and (c) is zero-to-tension stressing, $\sigma_{min} = 0$.

From Mechanical Behavior of Materials, Norman E. Dowling

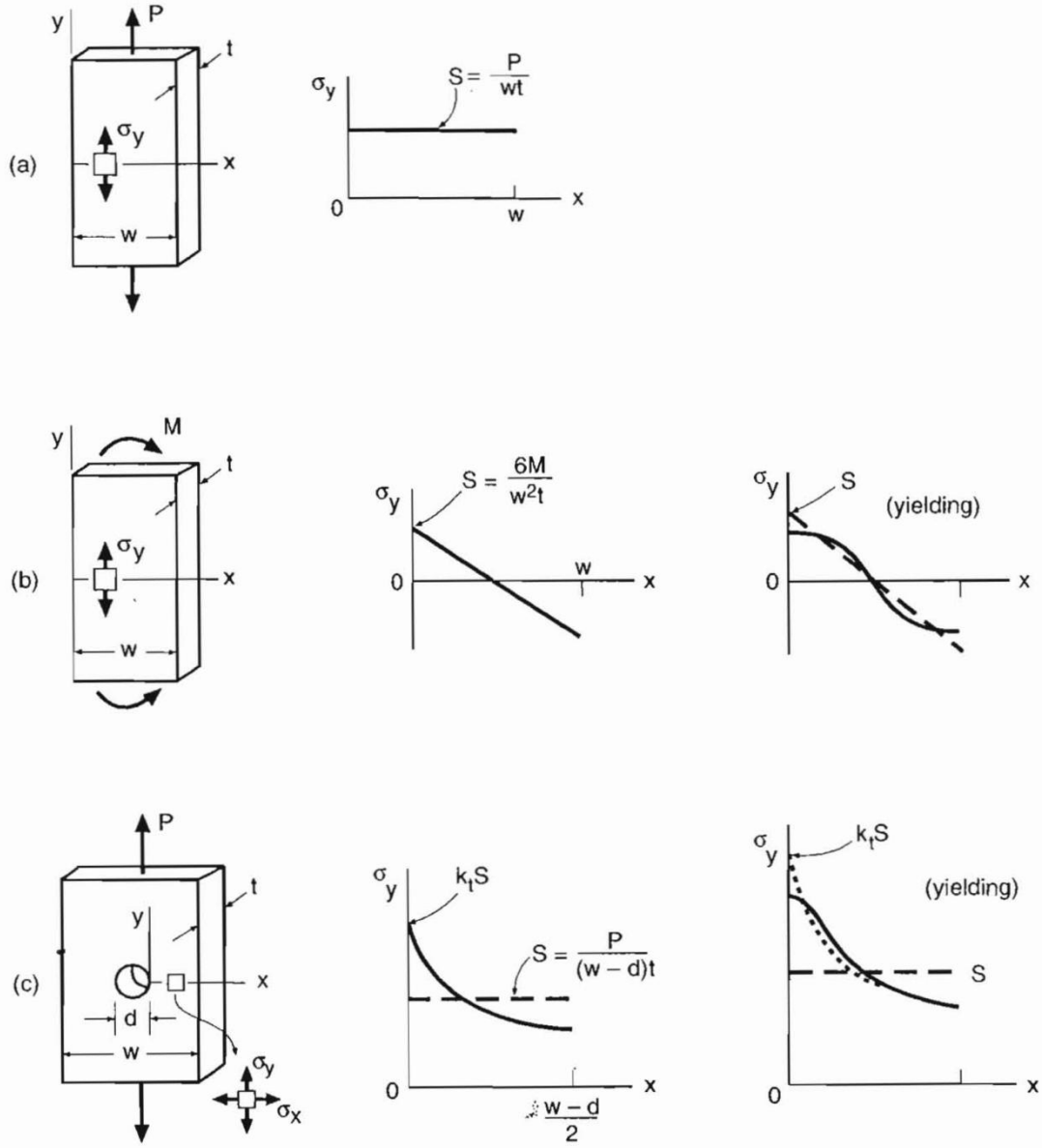

Figure 9.3 Actual and nominal stresses for (a) simple tension, (b) bending, and (c) a notched member. Actual stress distributions σ_y vs. x are shown as solid lines, and hypothetical distributions associated with nominal stresses S as dashed lines. In (c), the stress distribution that would occur if there were no yielding is shown as a dotted line.

From Mechanical Behavior of Materials, Norman E. Dowling

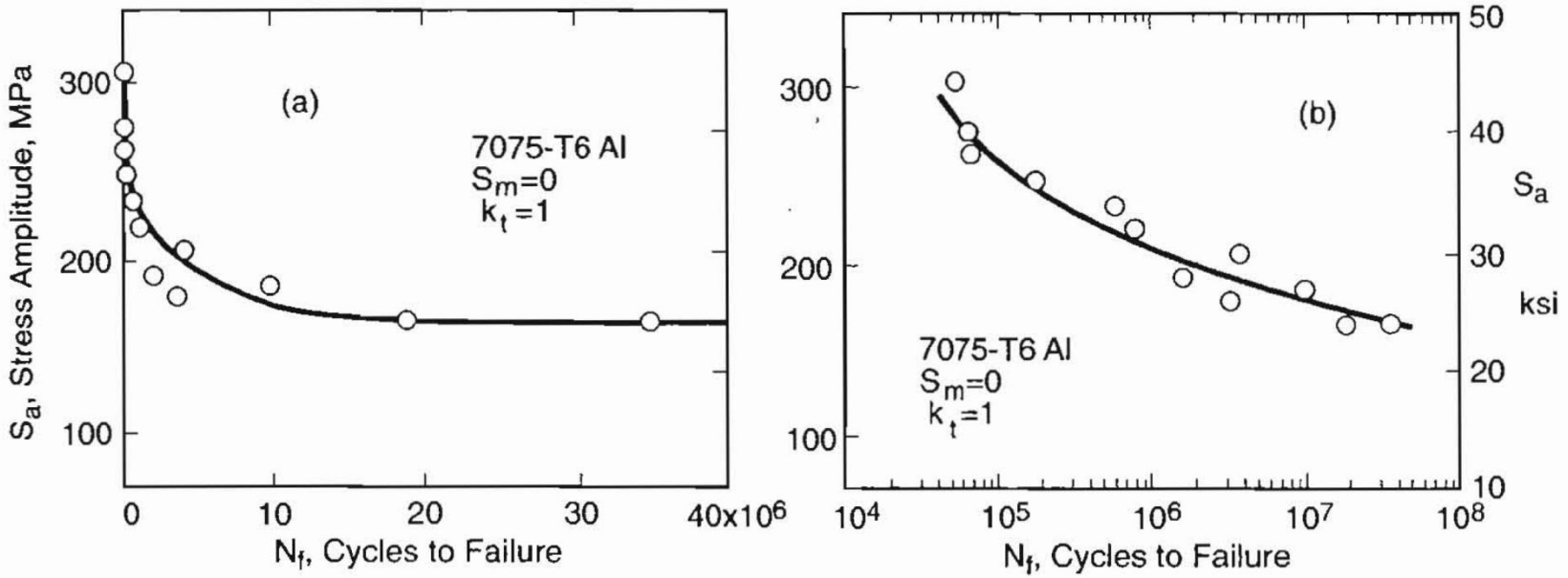

Figure 9.4 Stress versus life (*S-N*) curves from rotating bending tests of unnotched specimens of an aluminum alloy. Identical linear stress scales are used, but the cycle numbers are plotted on a linear scale in (a), and on a logarithmic one in (b). (Data from [MacGregor 52].)

From Mechanical Behavior
of Materials, Norman E. Dowling

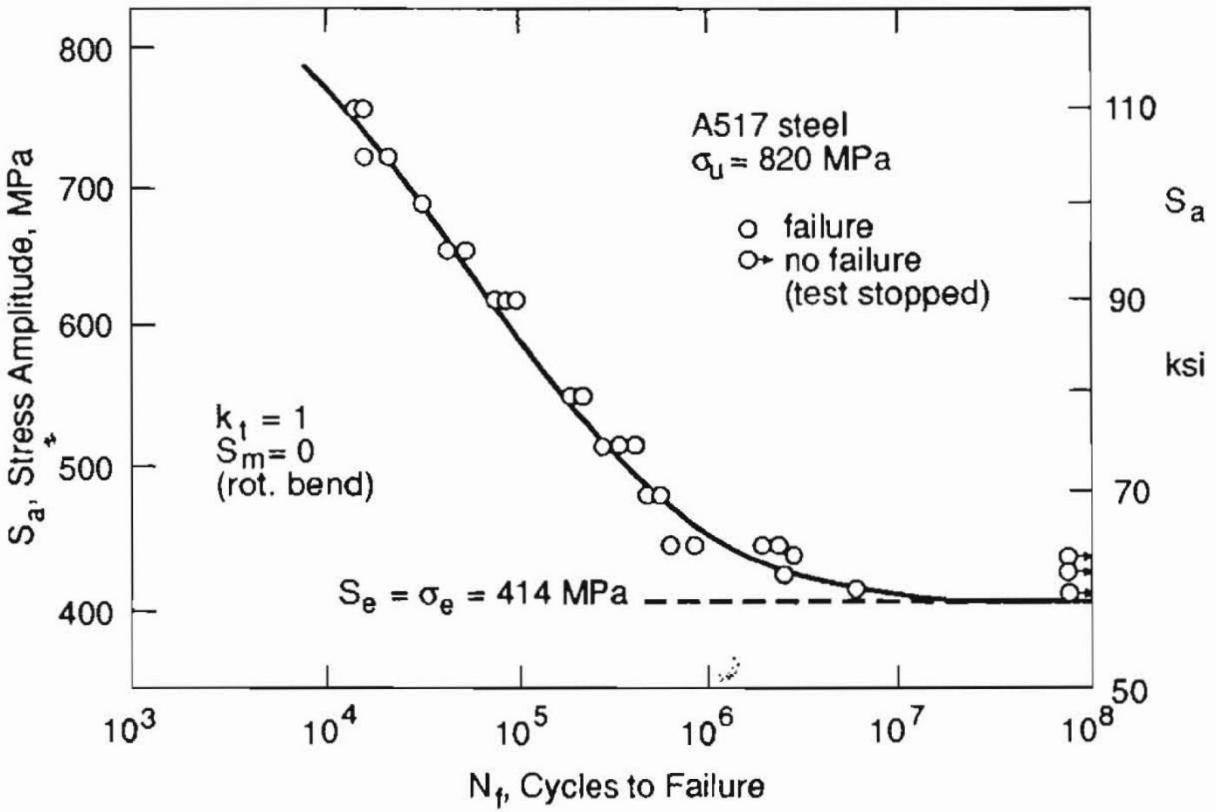

Figure 9.5 Rotating bending *S-N* curve for unnotched specimens of a steel with a distinct fatigue limit. (Adapted from [Brockenbrough 81]; used with permission.)

From Mechanical Behavior
of Materials, Norman E. Dowling

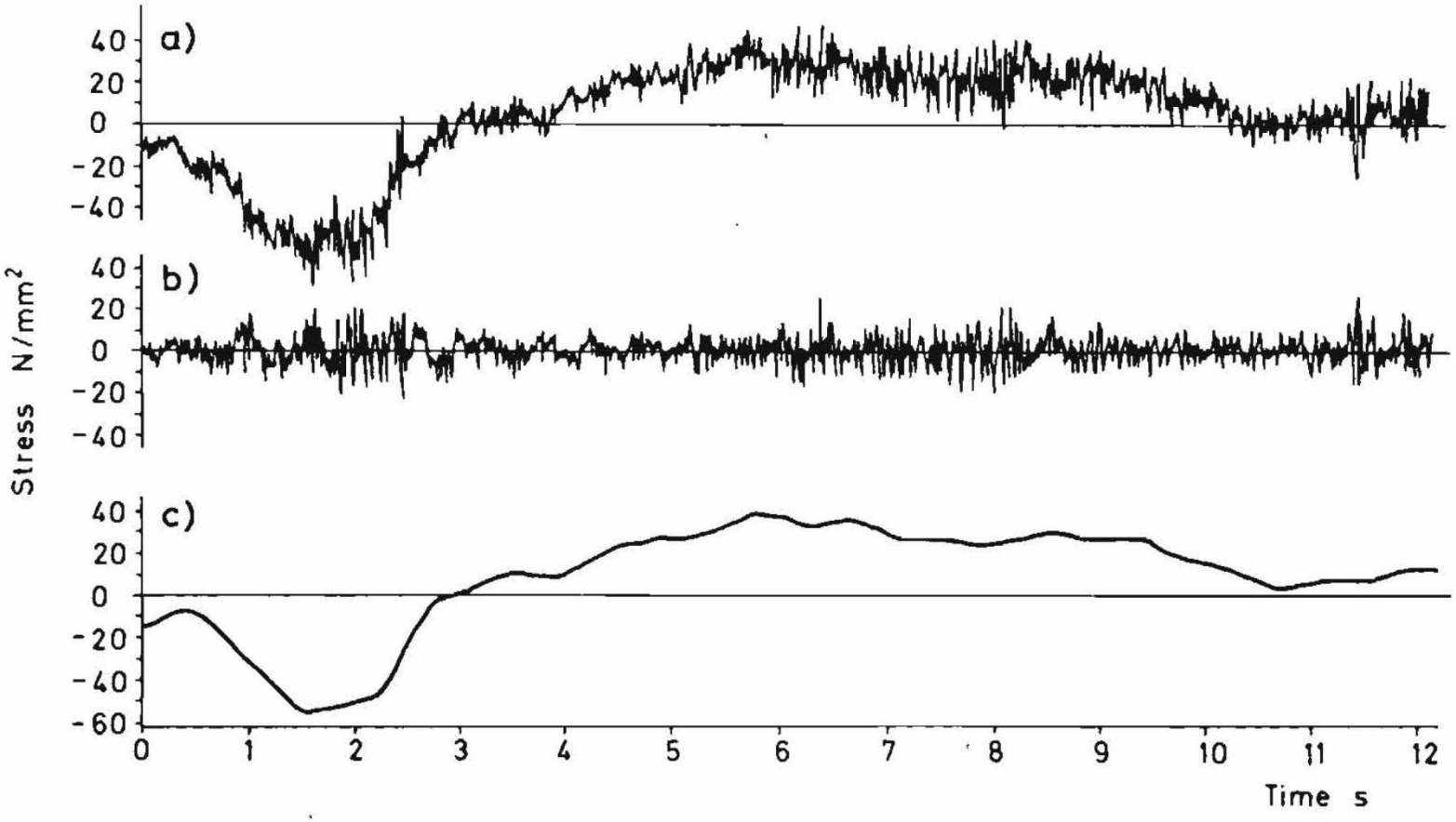

Figure 9.7 Sample record of stresses at the steering knuckle arm of a motor vehicle, including the original stress–time history (a), and the separation of this into the vibratory load due to roadway roughness (b) and the working load due to maneuvering the vehicle (c). (From [Buxbaum 73]; used with permission; first published by AGARD/NATO.)

From Mechanical Behavior of Materials, Norman E. Dowling

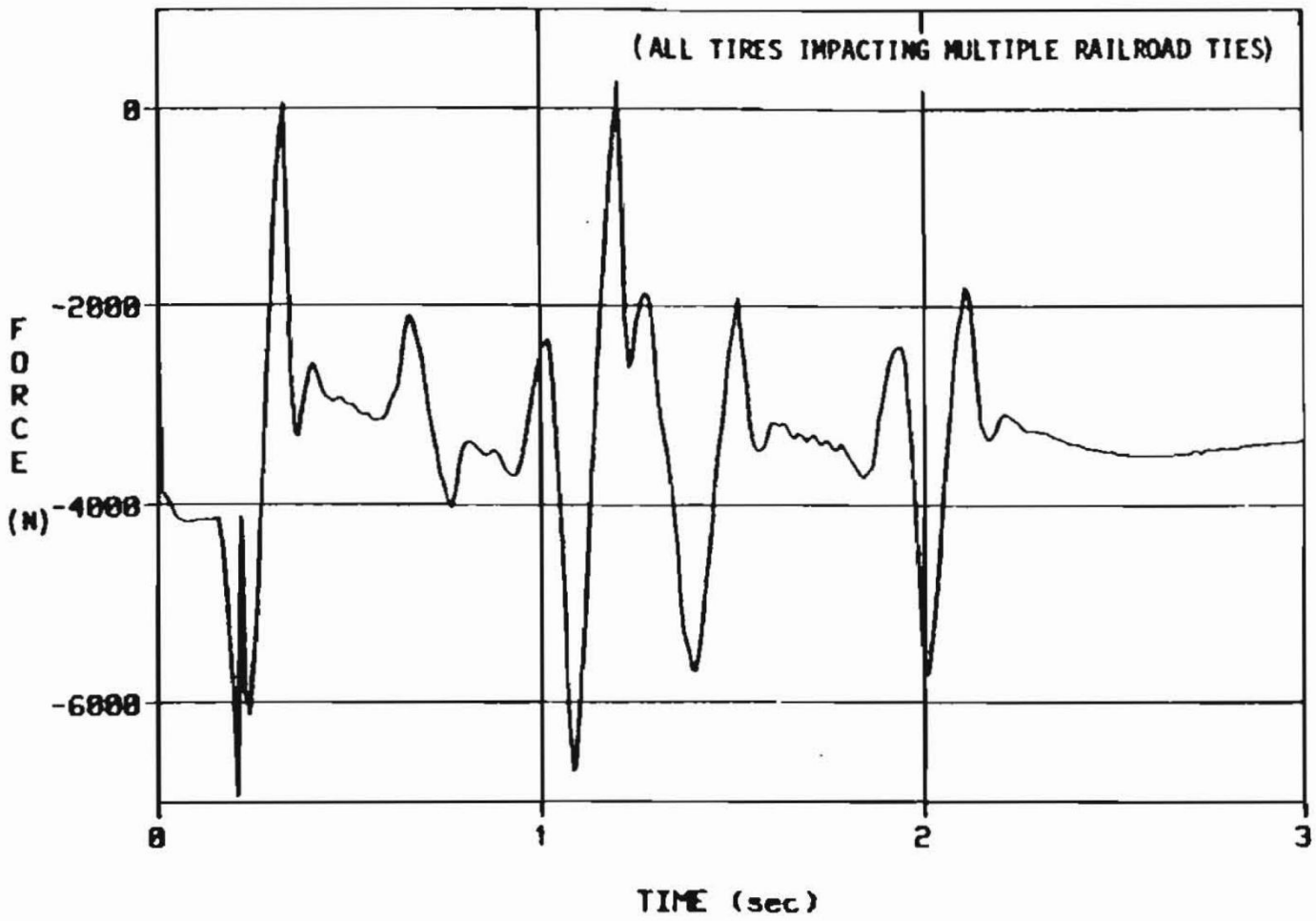

Figure 9.8 Calculated force on the front left lower ball joint in an automobile suspension, recorded while the tires were impacting railroad ties. (From [Thomas 87]; used with permission; © Society of Automotive Engineers.)

From Mechanical Behavior of Materials, Norman E. Dowling

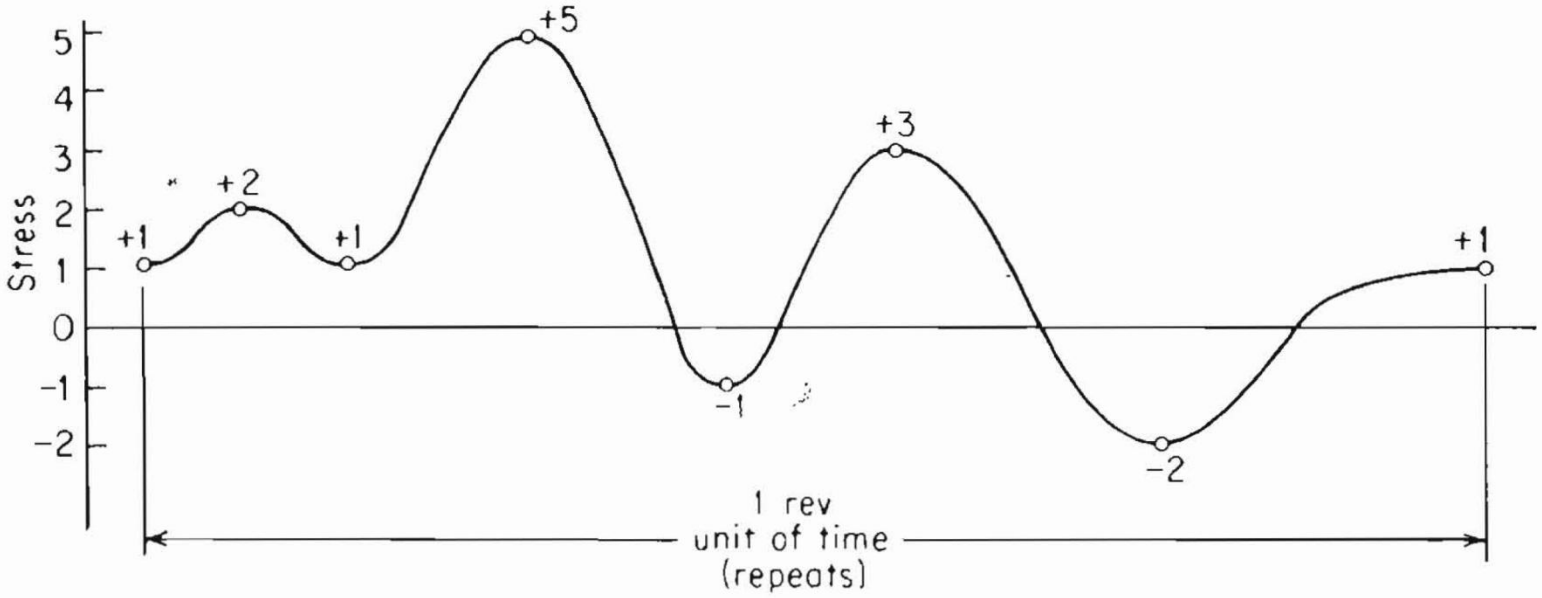

Figure 9.9 Loads during each revolution of a helicopter rotor. Feathering of the blade and interaction with the air cause these dynamic loads. (From [Boswell 59]; used with permission.)

From Mechanical Behavior
of Materials, Norman E. Dowling

Fatigue Testing: Rotating & Bending

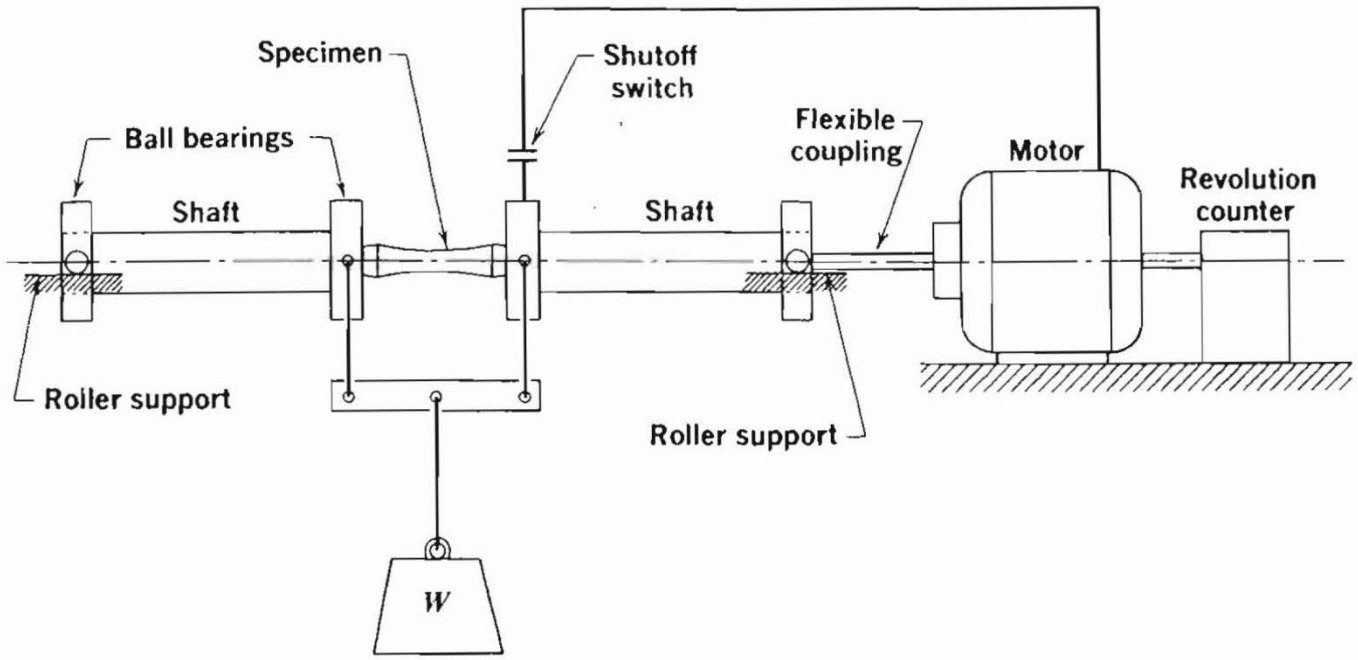

Figure 9.12 The R. R. Moore rotating beam fatigue testing machine. (From [Richards 61] p. 382; reprinted by permission of PWS-Kent Publishing Co., Boston.)

From Mechanical Behavior of Materials, Norman E. Dowling

Fatigue Testing: Reciprocating Cantilever Bending

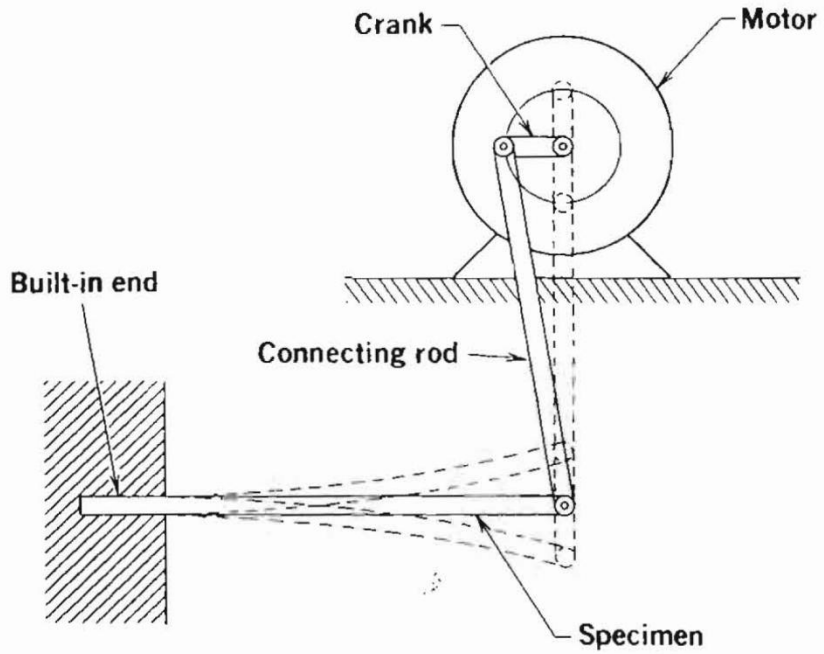

Figure 9.13 A reciprocating cantilever bending fatigue testing machine based on controlled deflections from a rotating eccentric. (From [Richards 61] p. 383; reprinted by permission of PWS-Kent Publishing Co., Boston.)

From Mechanical Behavior of Materials, Norman E. Dowling

Fatigue Test Specimens

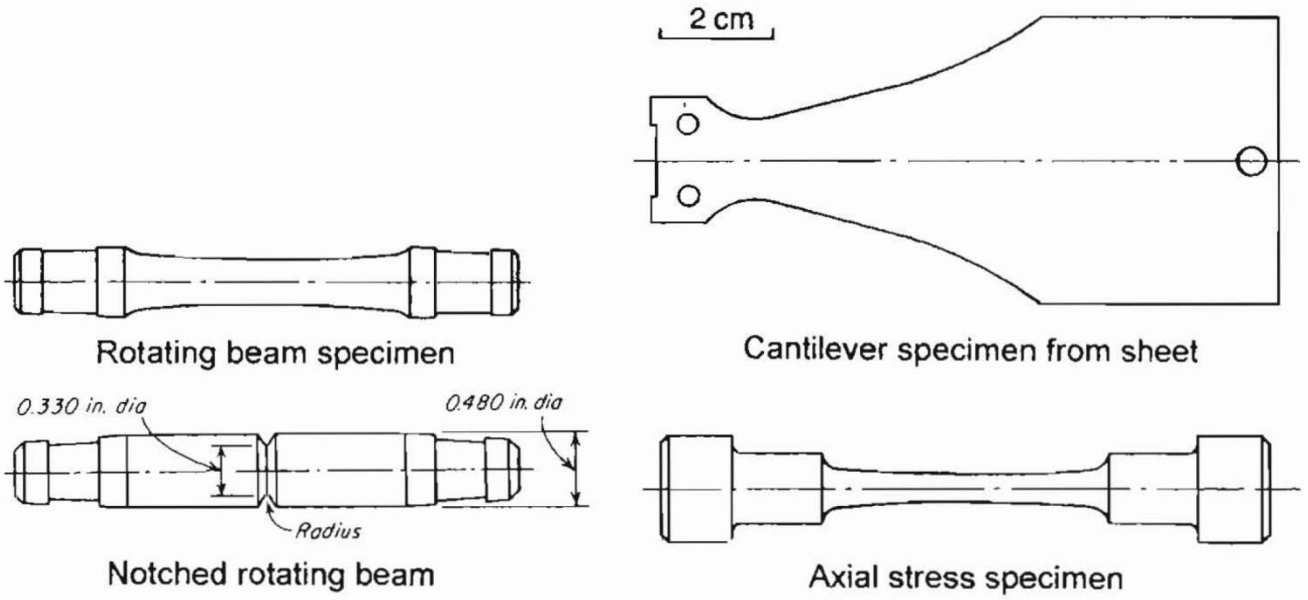

Figure 9.14 Various fatigue test specimens, all shown to the same scale. (Adapted from [Hartmann 59]; used with permission.)

From Mechanical Behavior of Materials, Norman E. Dowling

Fatigue Fractography

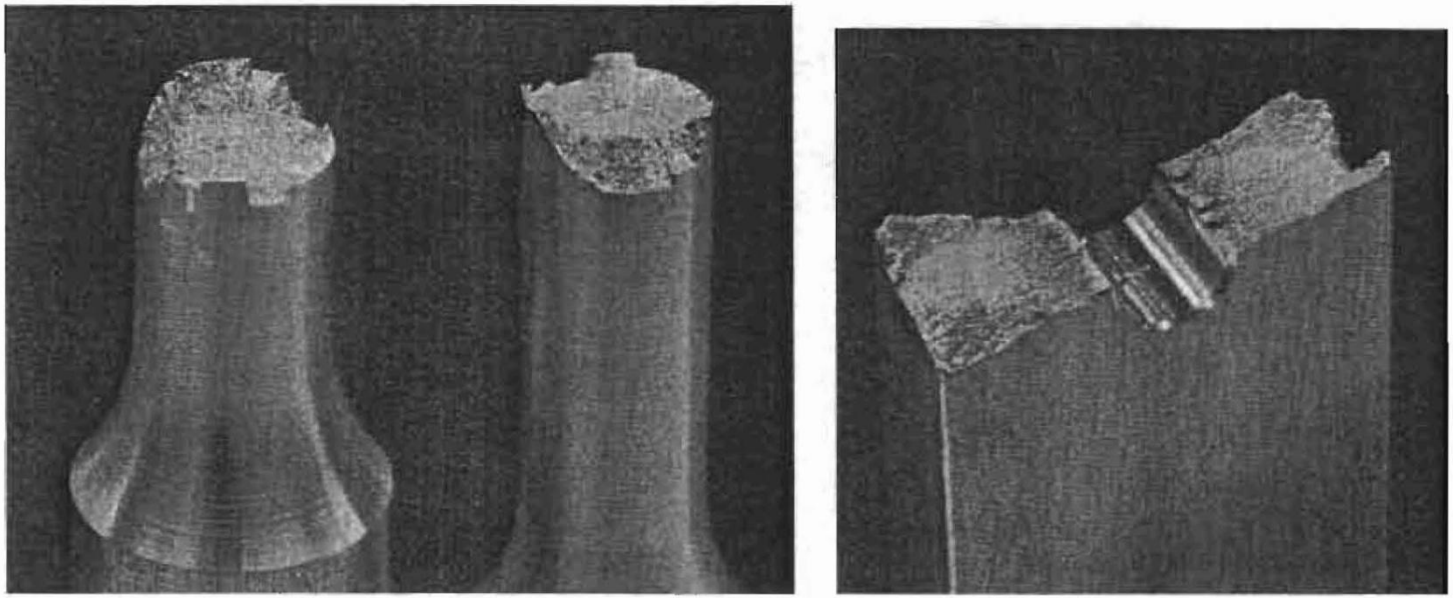

Figure 9.16 Photographs of broken 7075-T6 aluminum fatigue test specimens: unnotched axial specimen, 7.6 mm diameter (left); and plate 19 mm wide with a round hole (right). In the unnotched specimen, the crack started in the flat region with slightly lighter color, and cracks in the notched specimen started on each side of the hole. (Photos by R. A. Simonds.)

From Mechanical Behavior of Materials, Norman E. Dowling

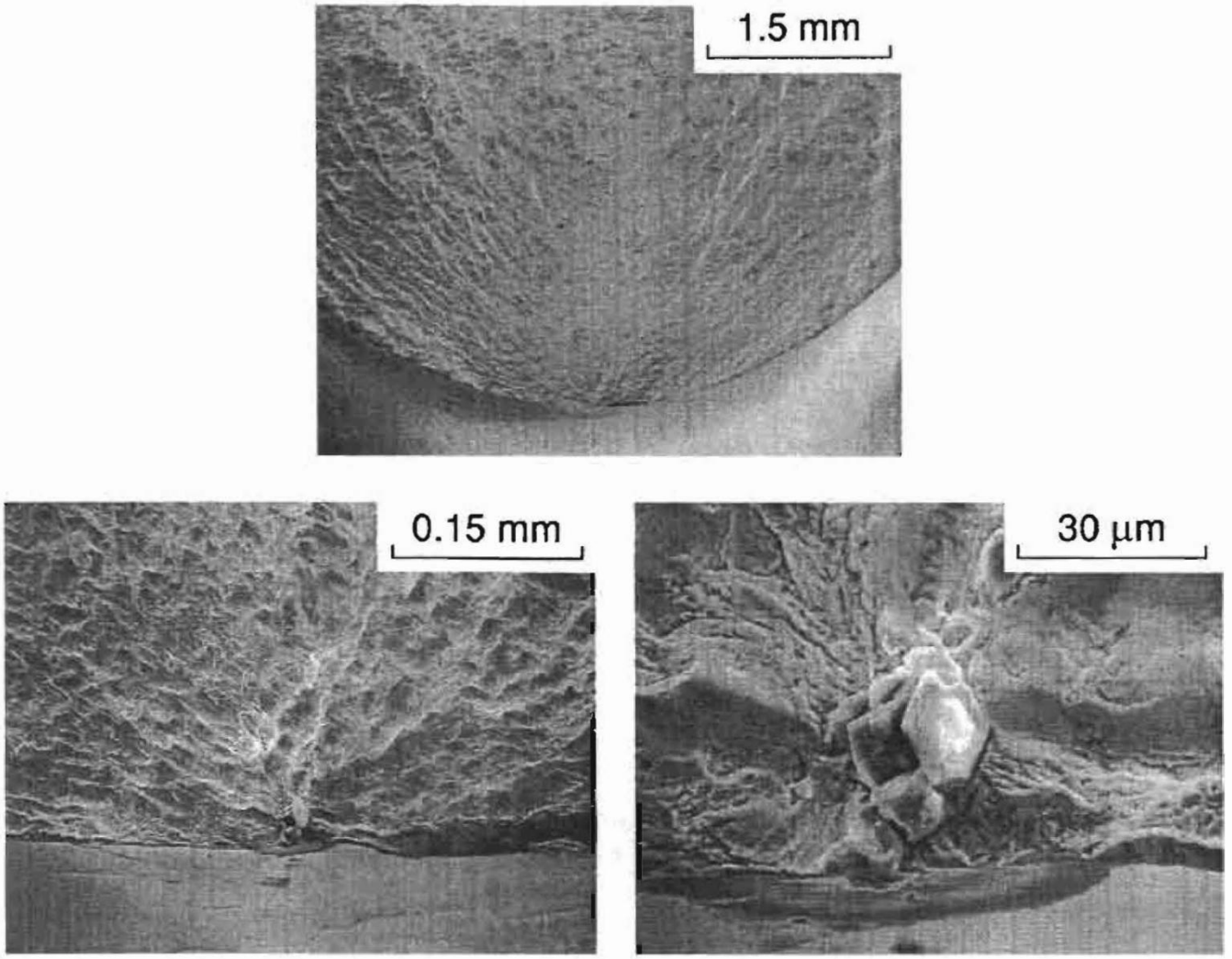

Figure 9.19 Fatigue crack origin in an unnotched axial test specimen of AISI 4340 steel having $\sigma_u = 780$ MPa, tested at $\sigma_a = 440$ MPa with $\sigma_m = 0$. The inclusion that started the crack can be seen at the two higher magnifications. (SEM photos by A. Madeyski, Westinghouse Science and Technology Ctr., Pittsburgh, PA; see [Dowling 83] for related data.)

From Mechanical Behavior of Materials, Norman E. Dowling

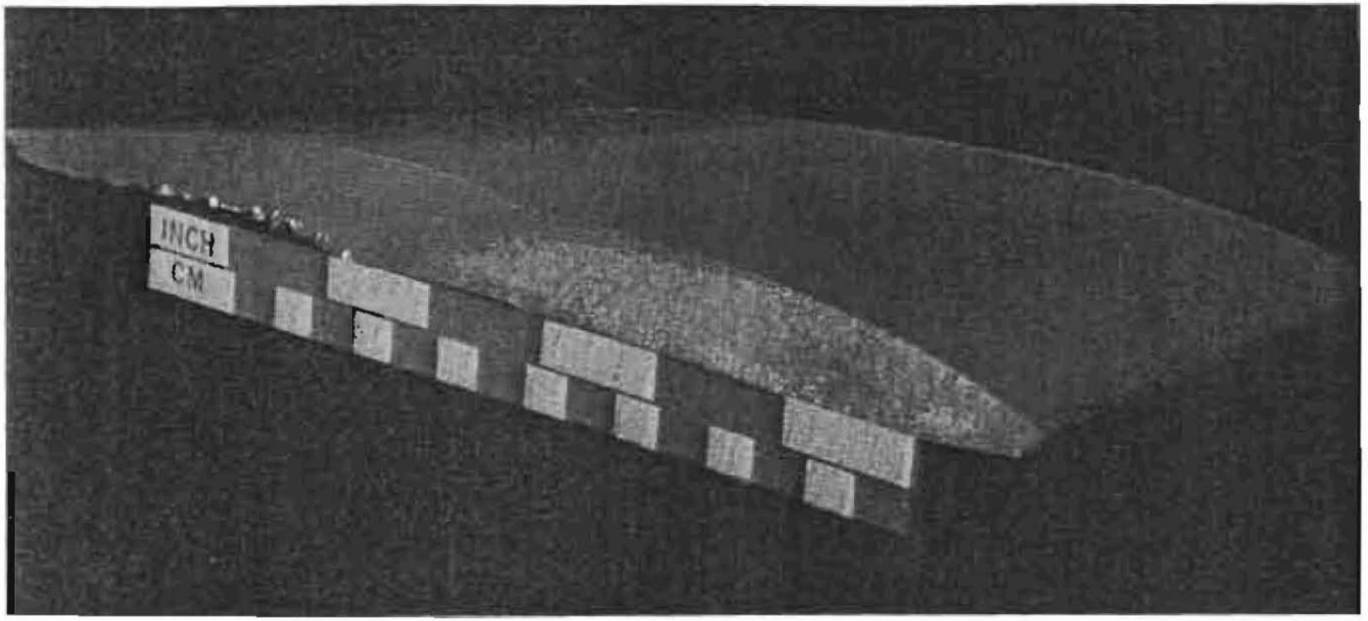

Figure 9.20 Fatigue failure of an aluminum alloy airplane propeller. The failure began at a small gouge on the bottom edge, approximately 2 cm from the right end of the scale. (Photo by R. A. Simonds; sample loaned for photo by Prof. J. L. Lytton of Virginia Tech, Blacksburg, VA.)

From Mechanical Behavior
of Materials, Norman E. Dowling

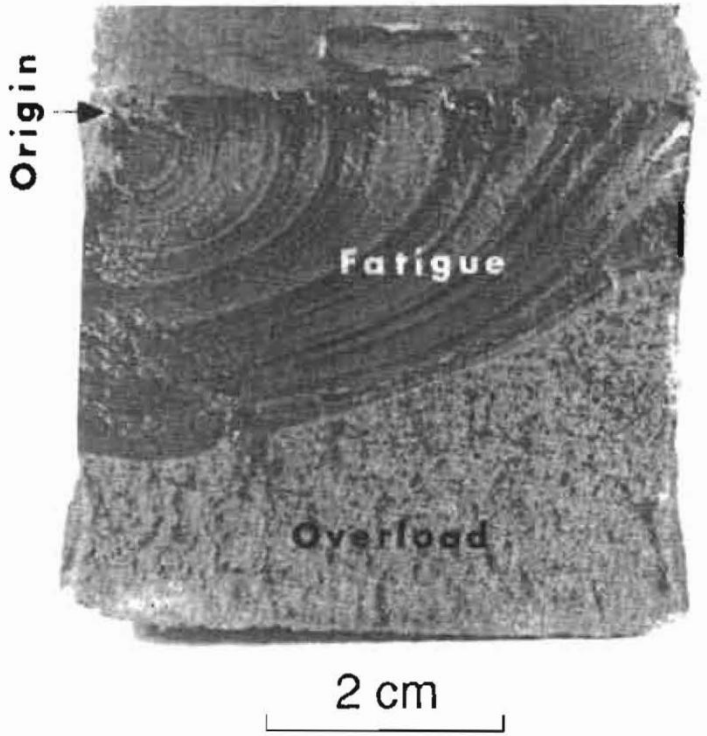

Figure 9.21 Fracture surfaces for fatigue and final brittle fracture in an 18 Mn steel member. (Photo courtesy of A. Madeyski, Westinghouse Science and Technology Ctr., Pittsburgh, PA.)

From Mechanical Behavior of Materials, Norman E. Dowling

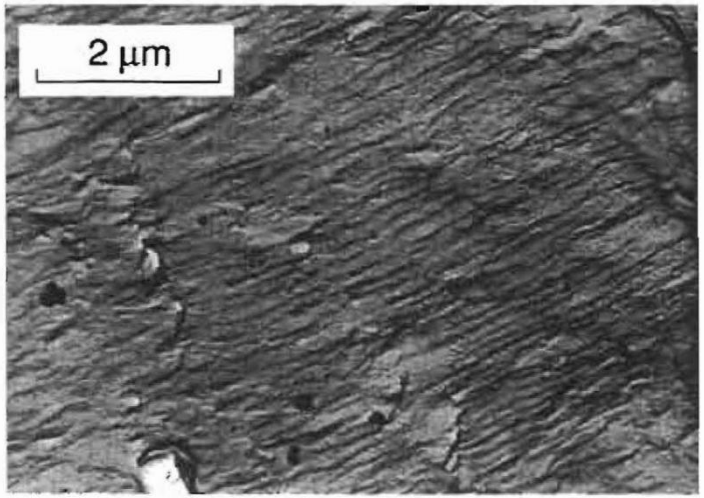

Figure 9.22 Fatigue striations spaced approximately 0.12 μm apart, from a fracture surface of a Ni-Cr-Mo-V steel. (Photo courtesy of A. Madeyski, Westinghouse Science and Technology Ctr., Pittsburgh, PA. Published in [Madeyski 78]; copyright © ASTM; reprinted with permission.)

From Mechanical Behavior
of Materials, Norman E. Dowling

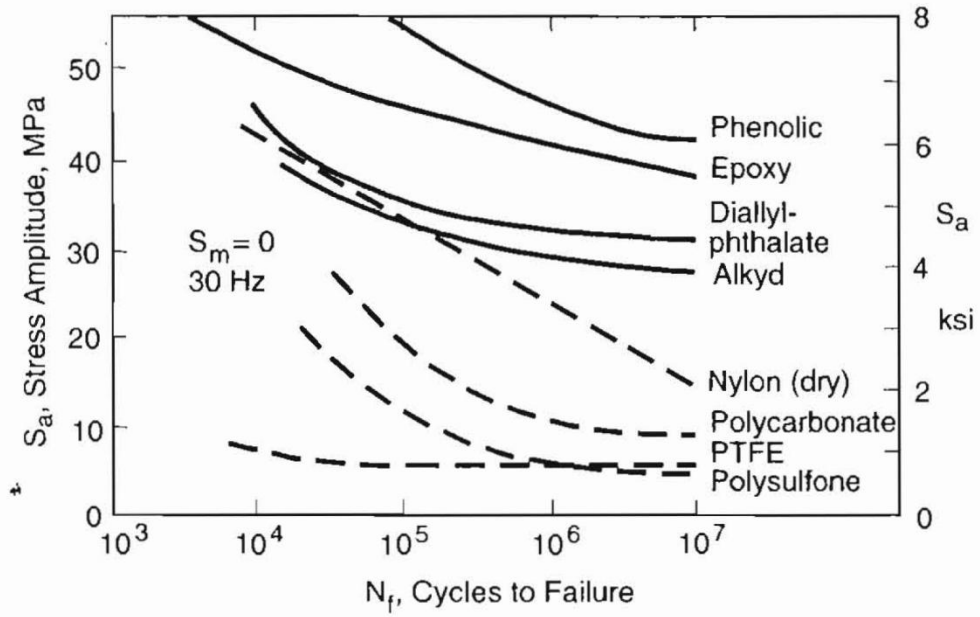

Figure 9.23 Stress–life curves from cantilever bending of mineral and glass-filled thermosets (solid lines) and unfilled thermoplastics (dashed lines). (Adapted from [Riddell 74]; used with permission.)

From Mechanical Behavior
of Materials, Norman E. Dowling

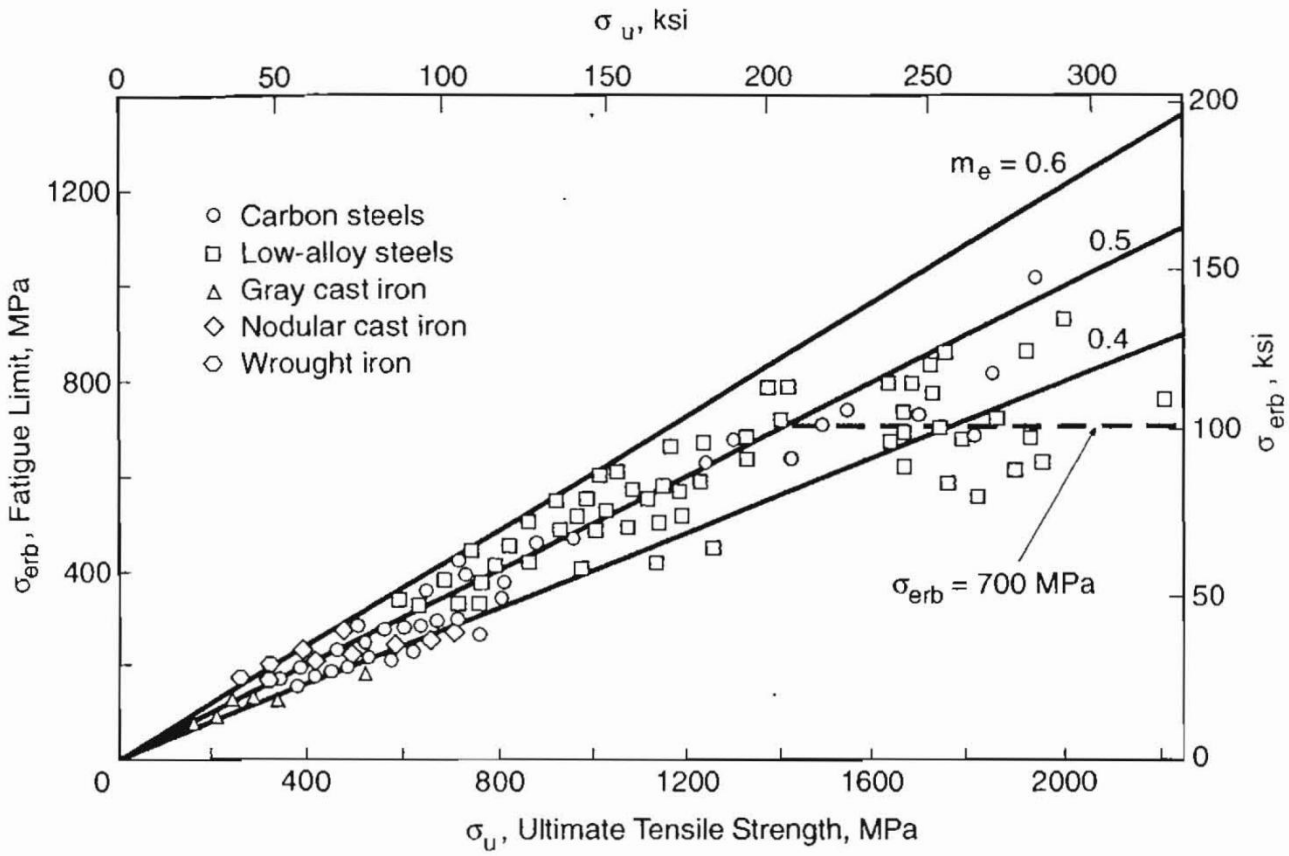

Figure 9.24 Rotating bending fatigue limits from polished specimens of various ferrous metals. The slopes $m_e = \sigma_{erb}/\sigma_u$ indicate the average and approximate extremes of the data for $\sigma_u < 1400$ MPa. (From data compiled by [Forrest 62].)

From Mechanical Behavior
of Materials, Norman E. Dowling

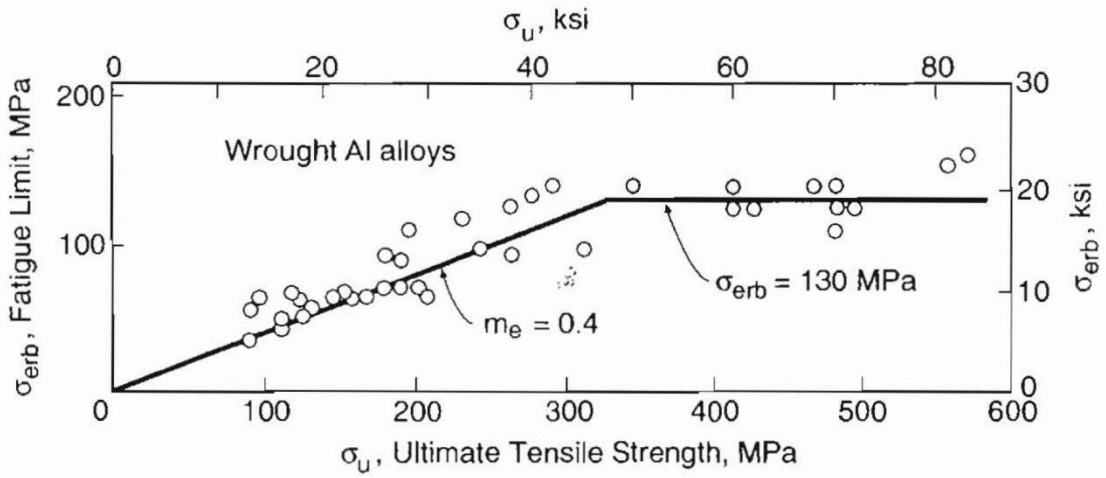

Figure 9.25 Fatigue strengths in rotating bending at 5×10^8 cycles for various tempers of common wrought aluminum alloys, including 1100, 2014, 2024, 3003, 5052, 6061, 6063, and 7075 alloys. The slope $m_e = \sigma_{erb}/\sigma_u$ indicates the average behavior for $\sigma_u < 325$ MPa. (Adapted from R. C. Juvinall, *Stress, Strain, and Strength*, 1967; [Juvinall 67] p. 215; reproduced with permission of the McGraw-Hill Companies.)

From Mechanical Behavior
of Materials, Norman E. Dowling

Effect of Mean Stress on Fatigue Life

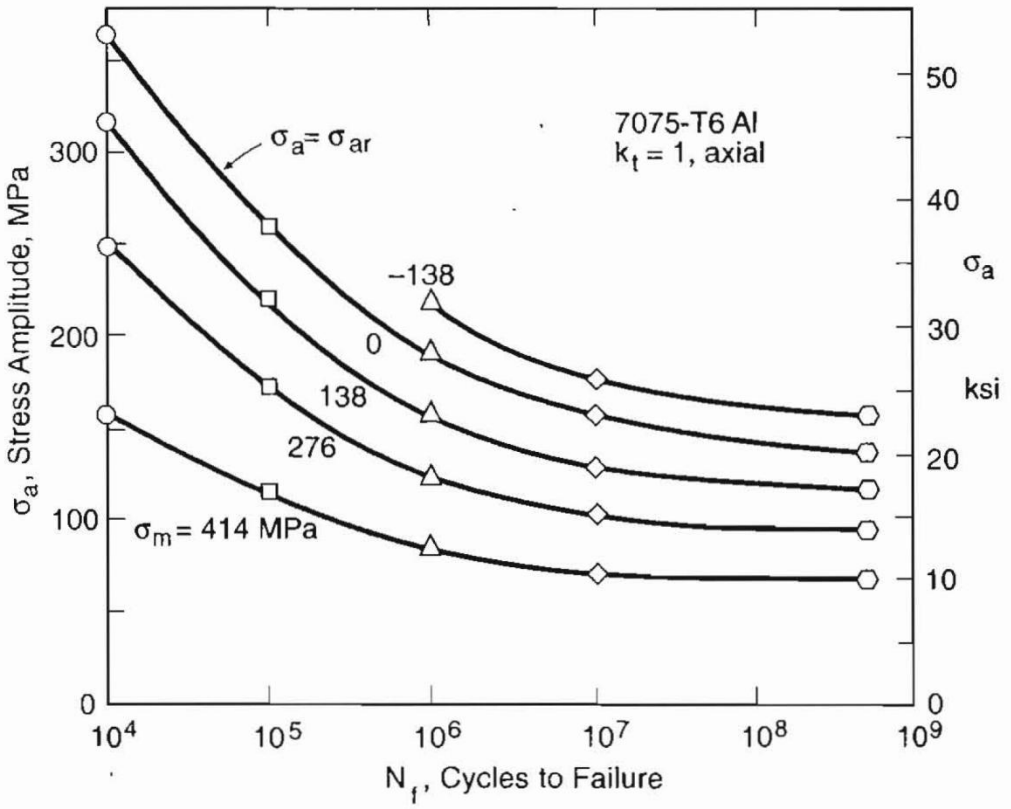

Figure 9.26 Axial loading *S-N* curves at various mean stresses for unnotched specimens of an aluminum alloy. The curves connect average fatigue strengths for a number of lots of material. (Data from [Howell 55].)

From Mechanical Behavior
of Materials, Norman E. Dowling

Effect of Notch on Fatigue Life

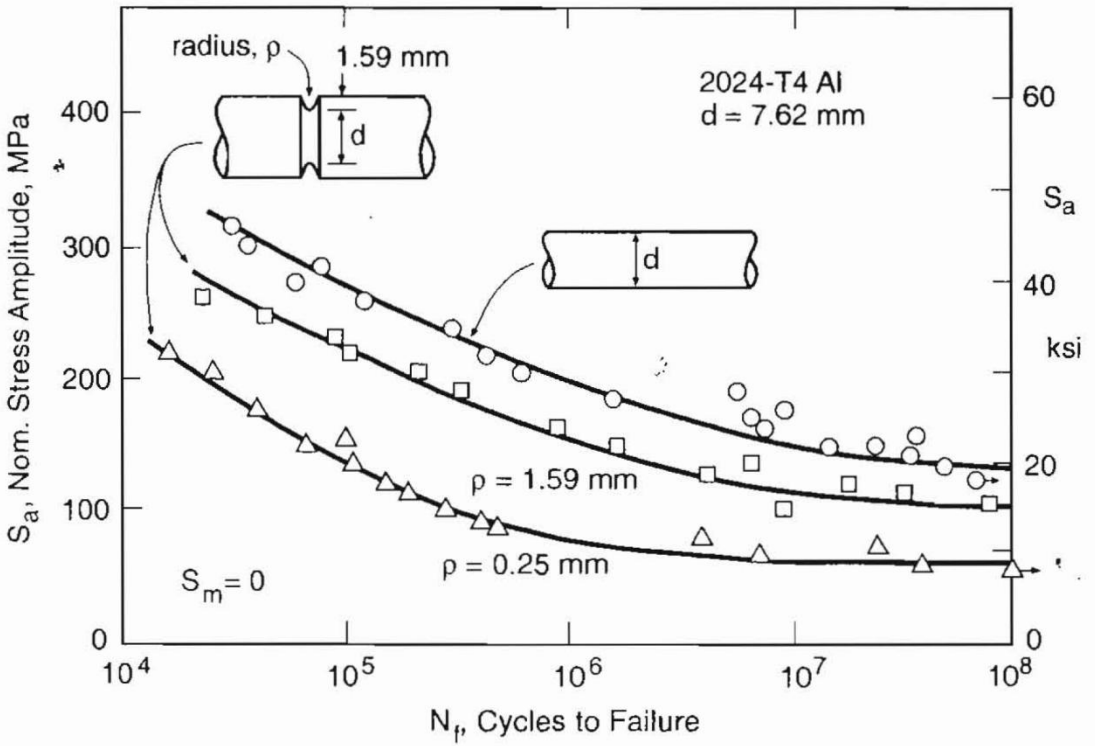

Figure 9.27 Effects of notches having $k_t = 1.6$ and 3.1 on rotating bending *S-N* curves of an aluminum alloy. (Adapted from [MacGregor 52].)

From Mechanical Behavior of Materials, Norman E. Dowling

Effect of Environment on Fatigue Life: Corrosion Fatigue

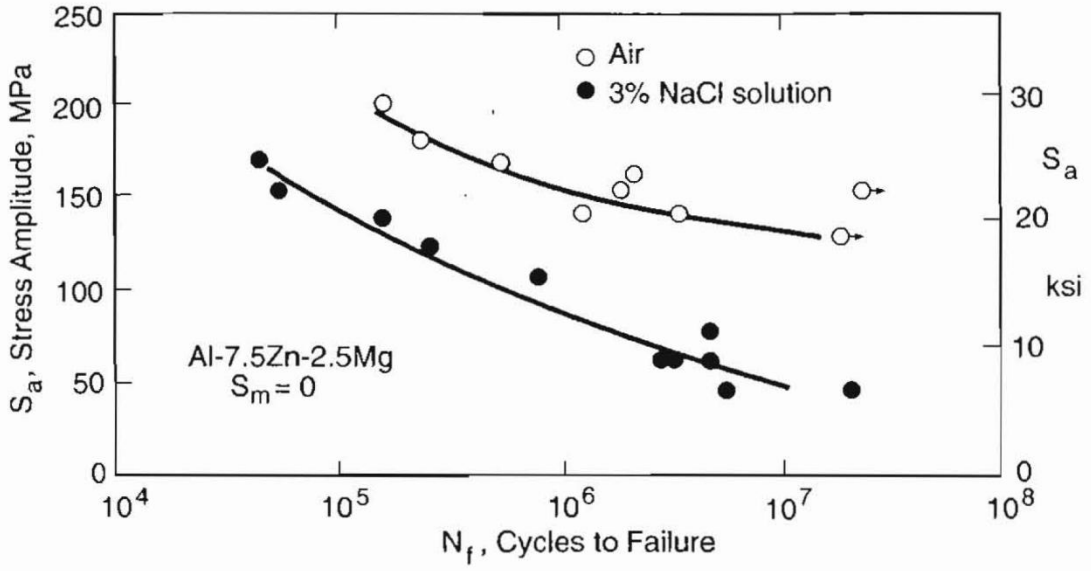

Figure 9.28 Effect of a salt solution similar to seawater on the bending fatigue behavior of an aluminum alloy. (Data from [Stubbington 61].)

From Mechanical Behavior of Materials, Norman E. Dowling

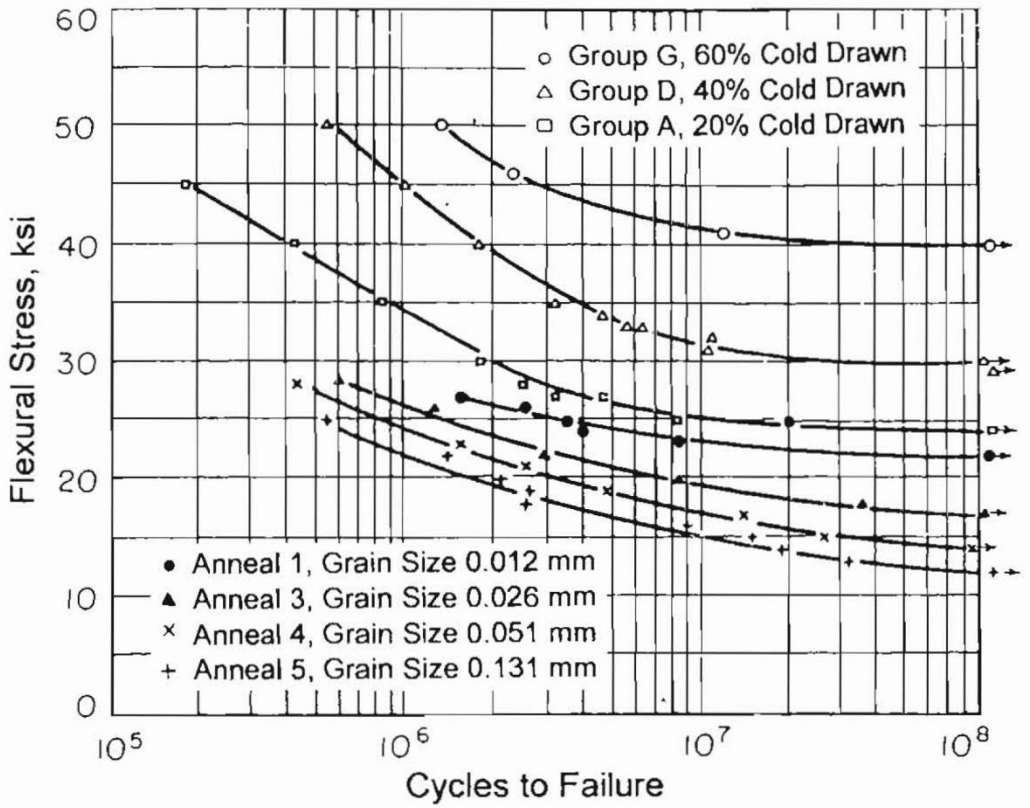

Figure 9.30 Influence of grain size and cold work on rotating bending *S-N* curves for 70Cu-30Zn brass. (From [Sinclair 52]; used with permission.)

From Mechanical Behavior of Materials, Norman E. Dowling

Effect of Residual Stress

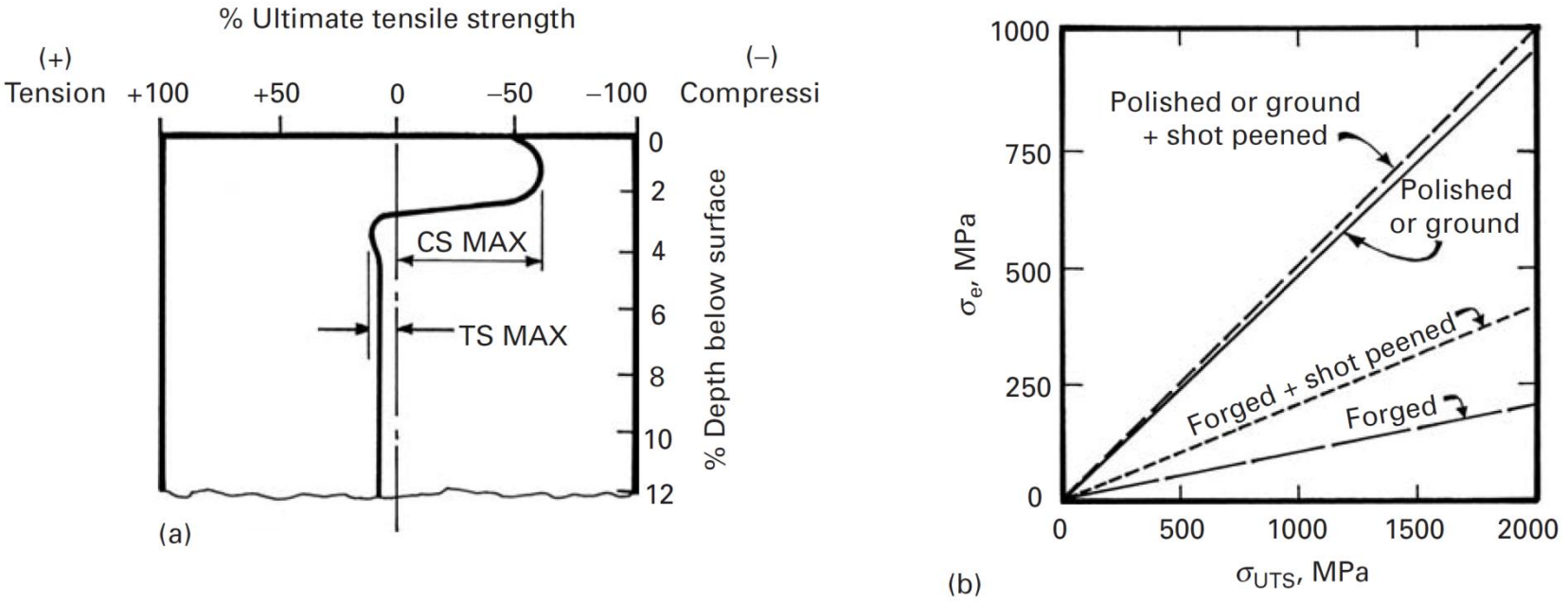

Fig. 14.15 (a) Residual stress profile generated by shot peening of a surface; CS and TS indicate compressive and tensile stress, respectively. (b) Effect of shot peening on fatigue life, *σe of steels* with different treatments as a fucntion of ultimate tensile strength, σ_{UTS}. *(After J. Y. Mann, Fatigue of Materials (Melbourne, Melbourne* University Press, 1967).)

Effect of Residual Stress

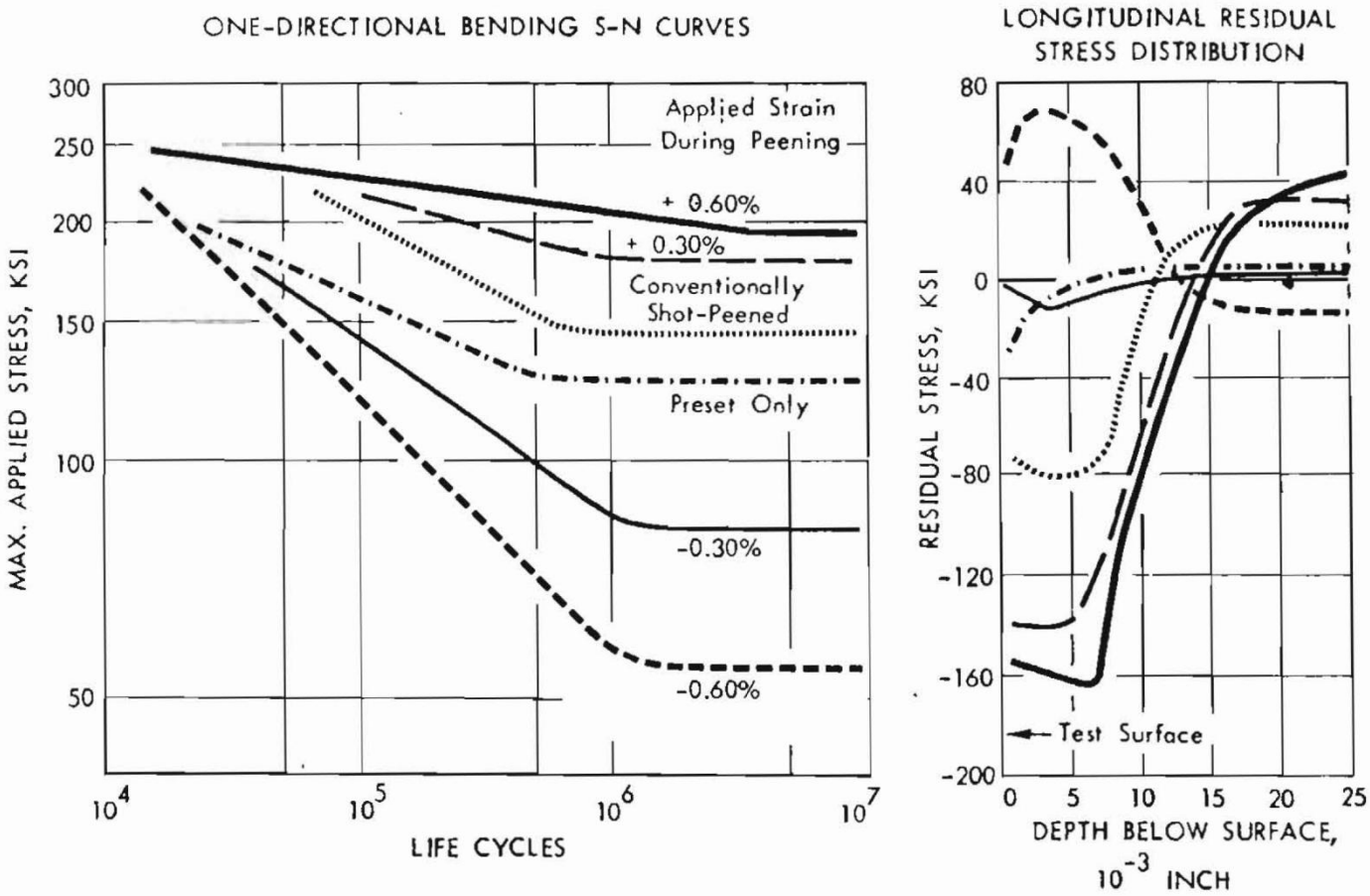

Figure 9.31 *S-N* curves for zero-to-maximum bending, and residual stresses, for variously shot peened steel leaf springs. (From [Mattson 59]; courtesy of General Motors Research Laboratories.)

From Mechanical Behavior of Materials, Norman E. Dowling

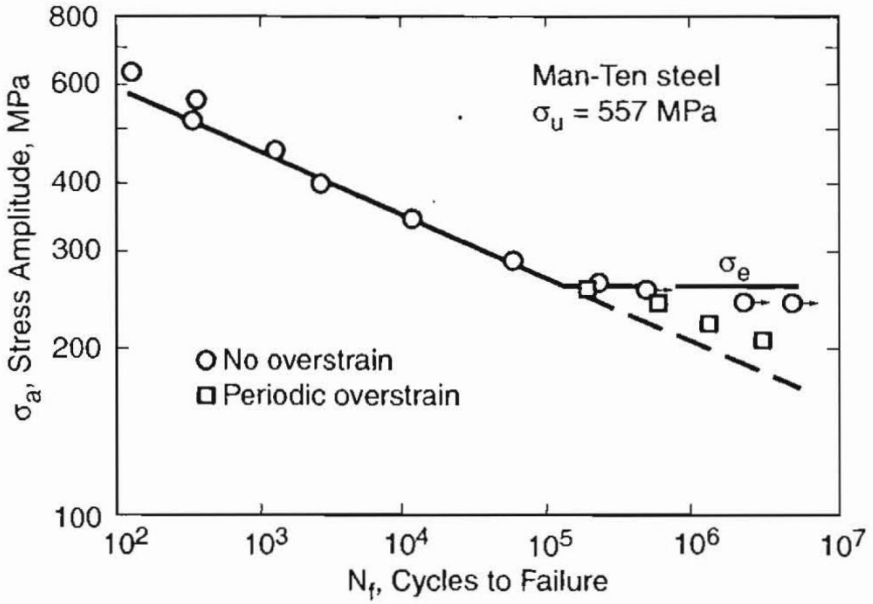

Figure 9.33 Stress–life data for a low-strength steel tested under constant amplitude cycling with zero mean stress. Periodic overstrain tests included severe cycles applied every 10^5 cycles, but with their $\Sigma N/N_f$ not exceeding a few percent. (Data from [Brose 74].)

From Mechanical Behavior
of Materials, Norman E. Dowling

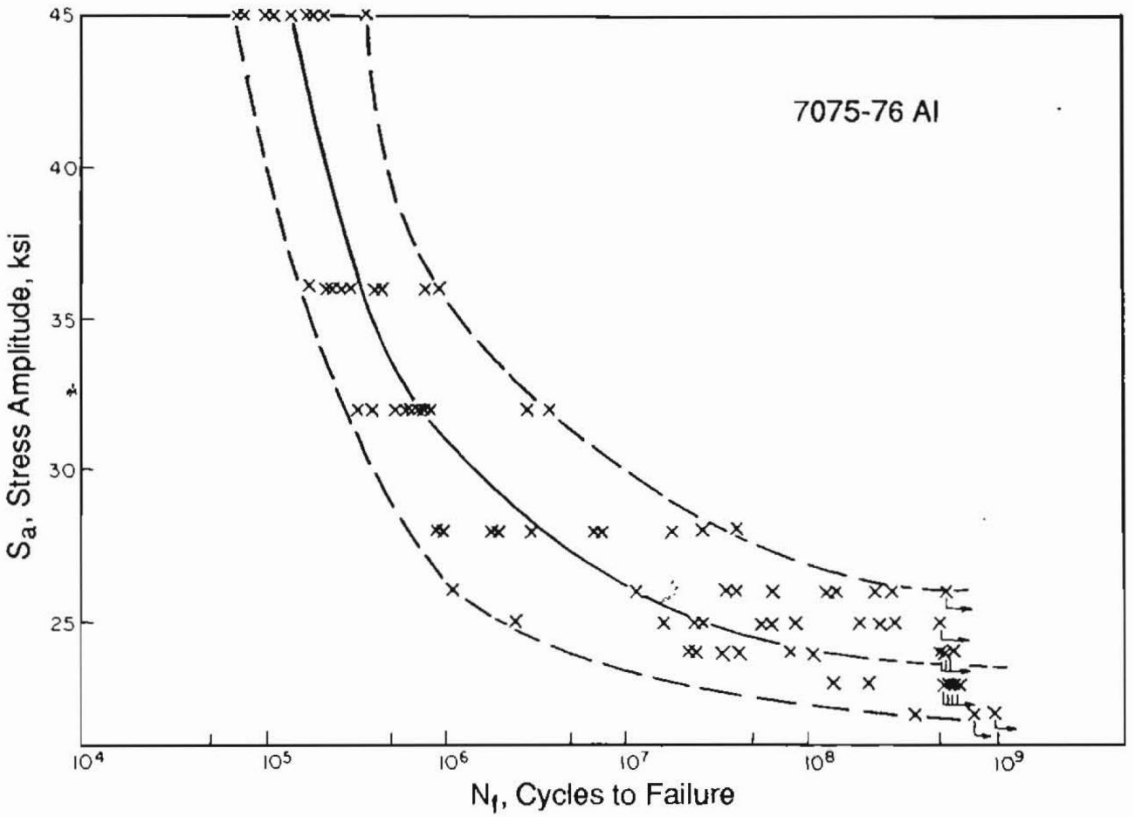

Figure 9.34 Scatter in rotating bending *S-N* data for an unnotched aluminum alloy. (Adapted from [Grover 66] p. 44.)

From Mechanical Behavior of Materials, Norman E. Dowling

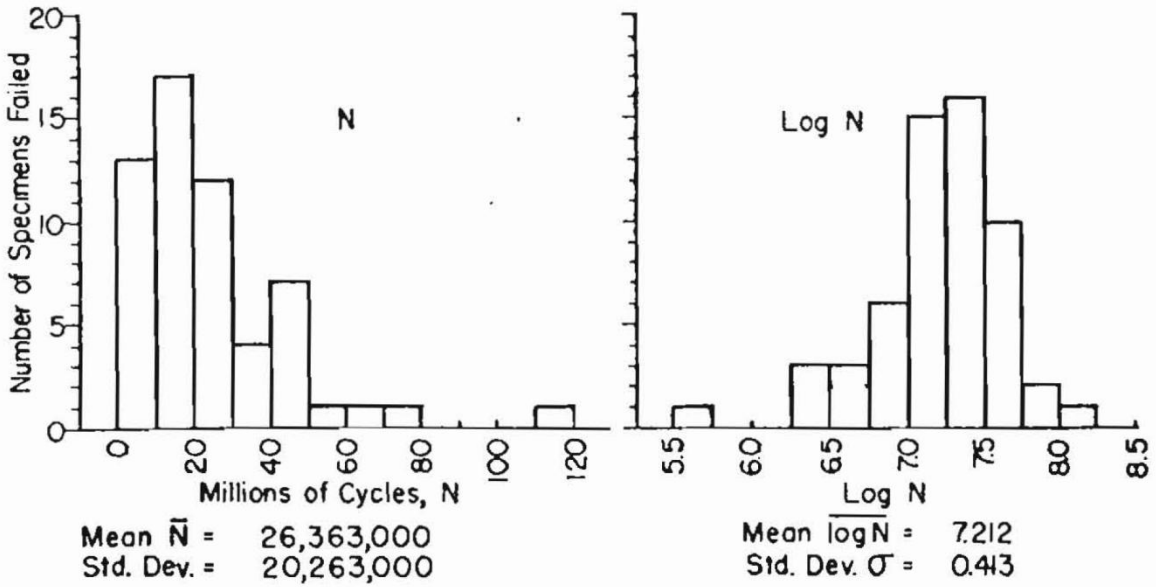

Figure 9.35 Distribution of fatigue lives for 57 small specimens of 7075-T6 aluminum tested at $S_a = 207$ MPa (30 ksi) in rotating bending. (From [Sinclair 53]; used with permission of ASME.)

From Mechanical Behavior
of Materials, Norman E. Dowling

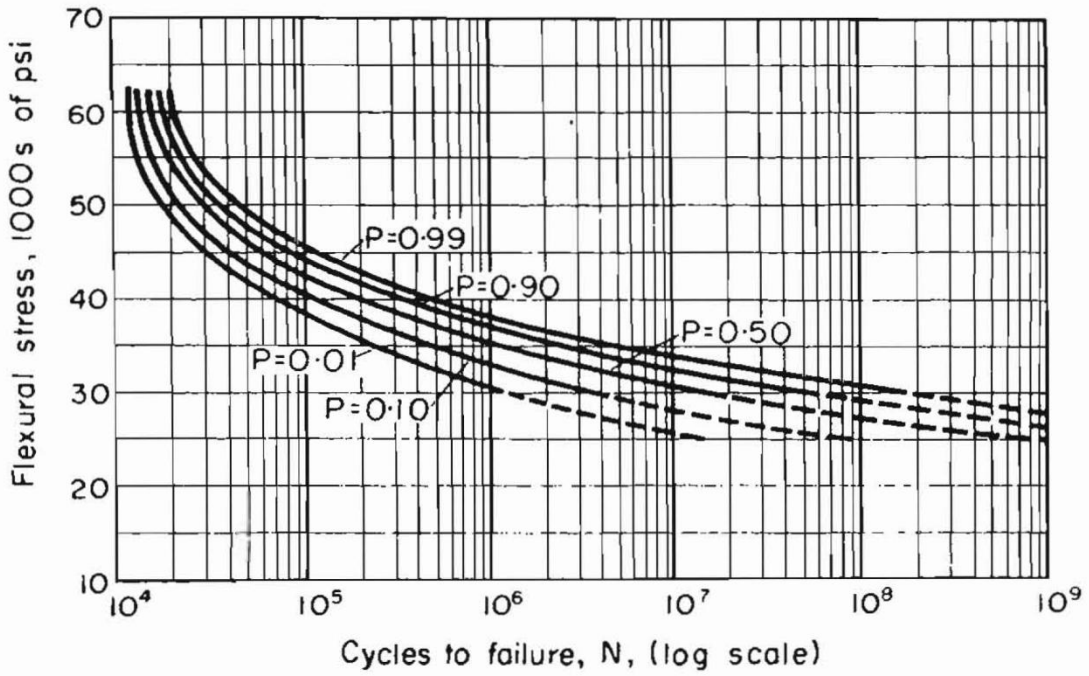

Figure 9.36 Family of rotating bending *S-N* curves for various probabilities of failure, *P*, from data for small unnotched specimens of 7075-T6 aluminum. (From [Sinclair 53]; used with permission of ASME.)

From Mechanical Behavior
of Materials, Norman E. Dowling

Goodman's relationship

$\sigma_a = \sigma_0[1 - \sigma_m/\sigma_{UTS}]$.

Gerber's relationship

$\sigma_a = \sigma_0[1 - (\sigma_m/\sigma_{UTS})^2]$

Soderberg's relationship

$\sigma_a = \sigma_0[1 - \sigma_m/\sigma_y]$.

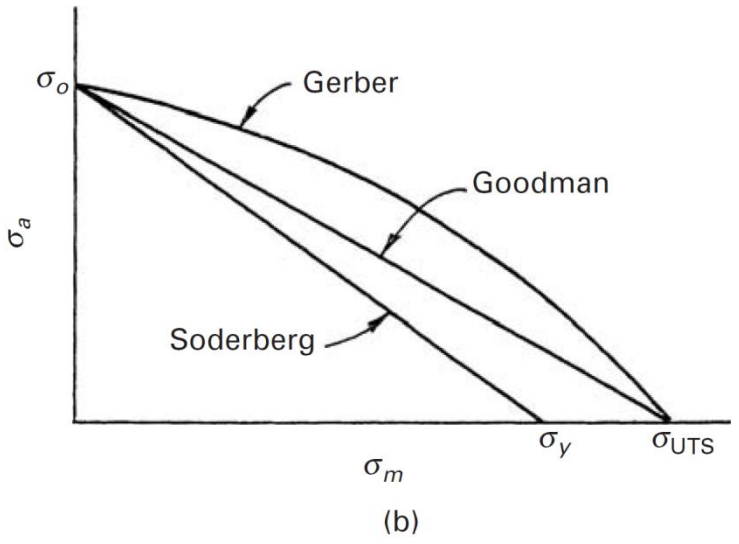

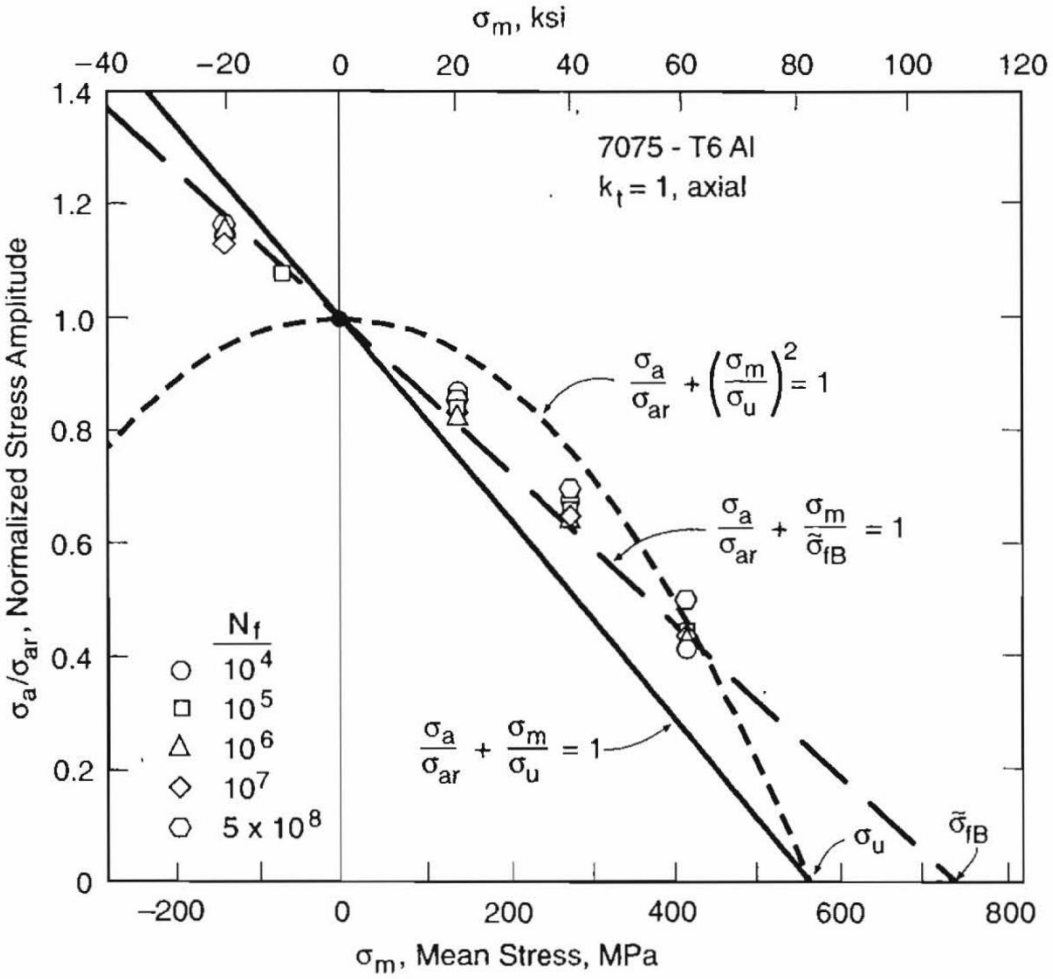

Figure 9.39 Normalized amplitude-mean diagram for 7075-T6 aluminum based on Fig. 9.37.

From Mechanical Behavior of Materials, Norman E. Dowling

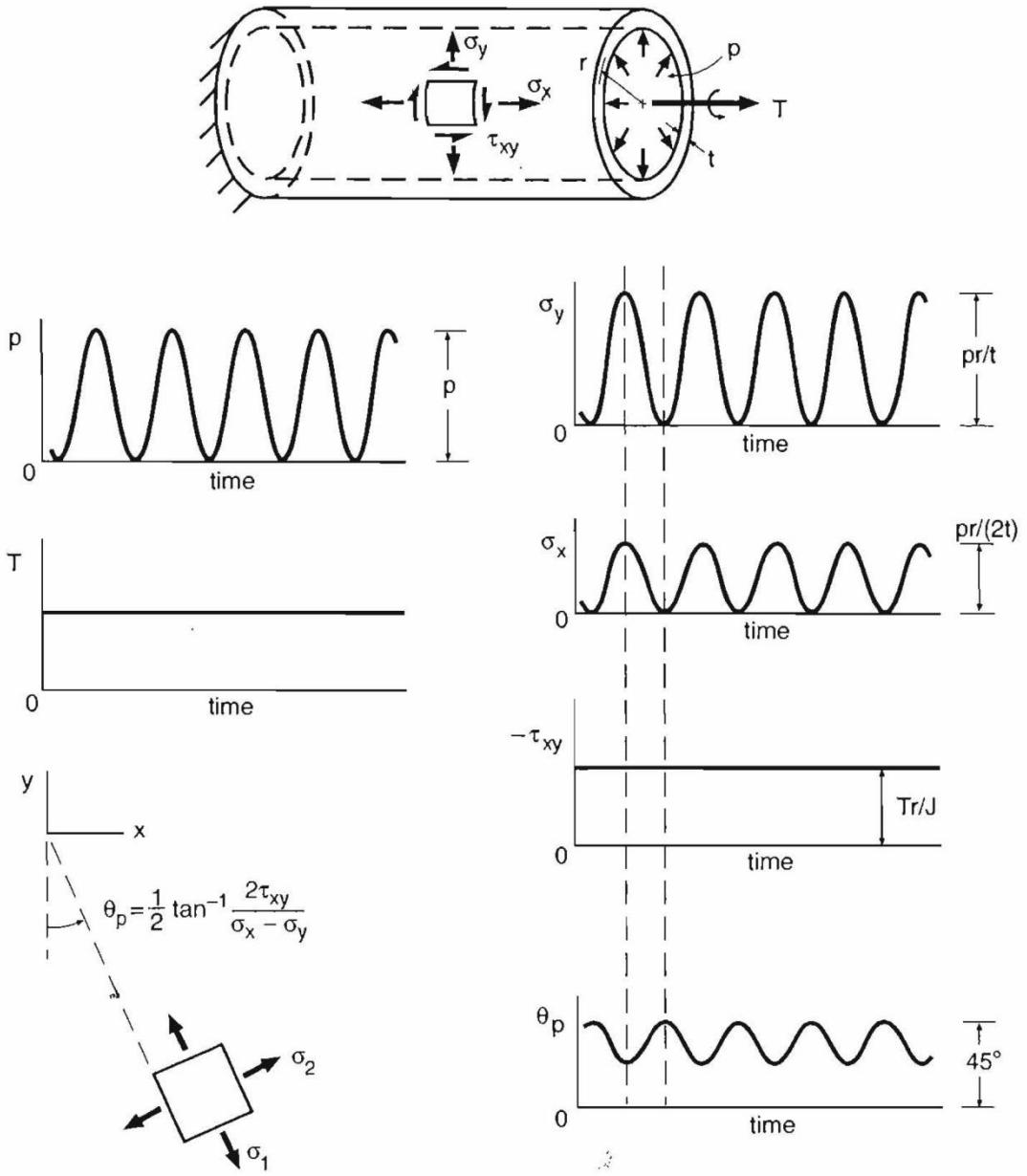

Figure 9.41 Combined cyclic pressure and steady torsion of a thin-walled tube with closed ends. The principal directions oscillate during each cycle.

From Mechanical Behavior of Materials, Norman E. Dowling

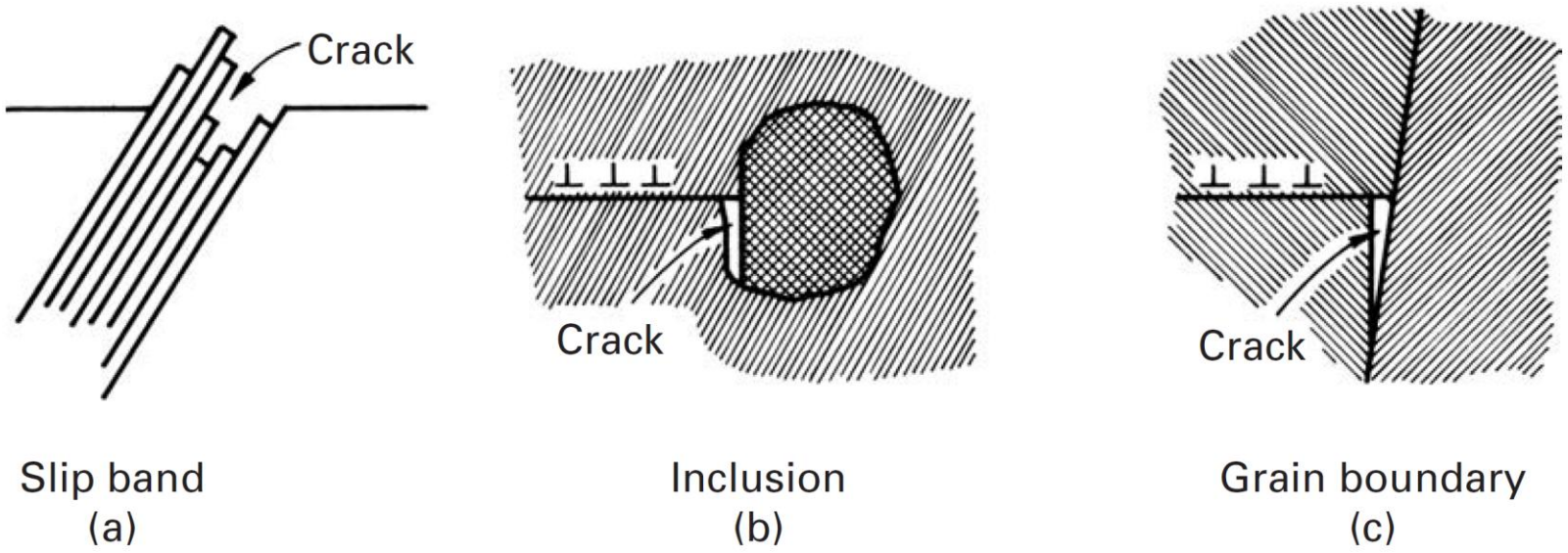

Fig. 14.14 Some mechanisms of fatigue crack nucleation.
(After J. C. Grosskreutz, *Tech. Rep. AFML-TR-70–55 (Wright*–Patterson AFB, OH: Air Force Materials Laboratory), 1970.)

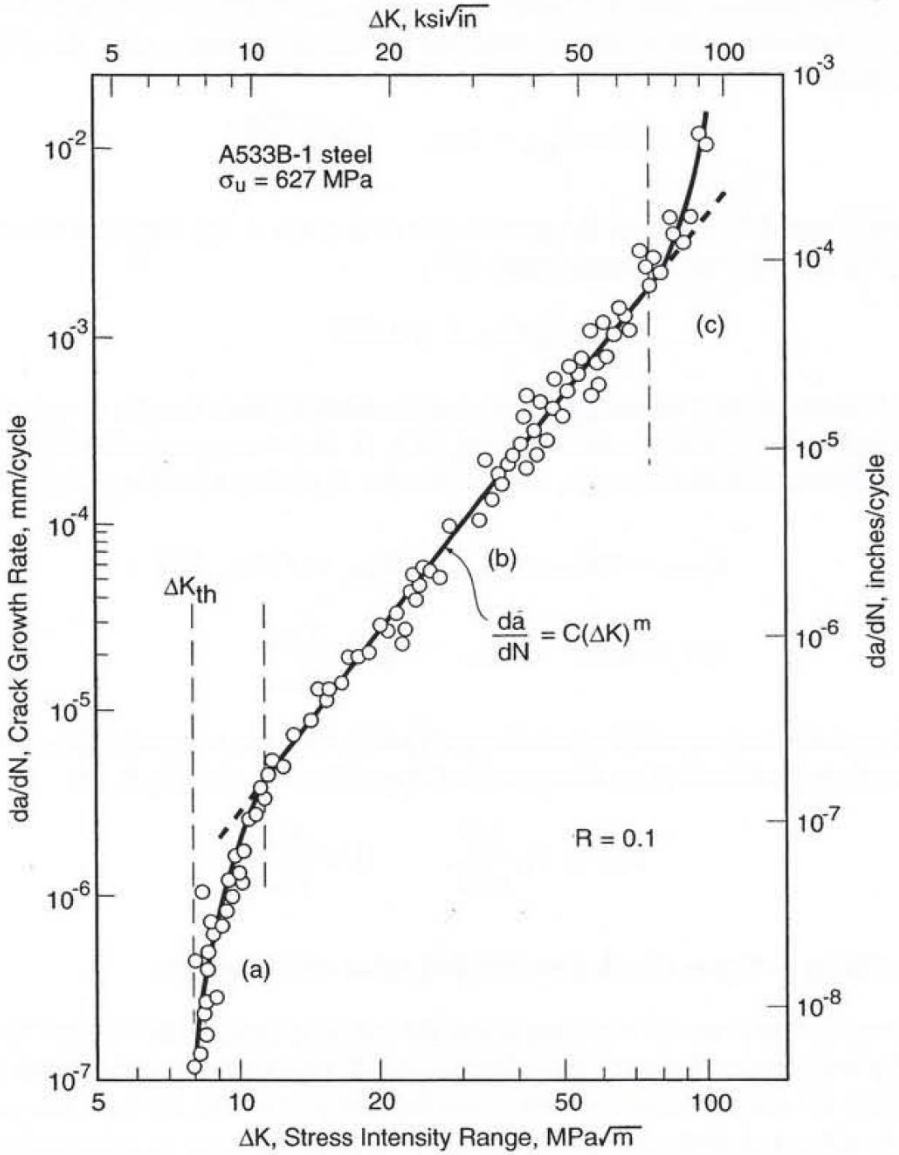

Figure 11.3 Fatigue crack growth rates over a wide range of stress intensities for a ductile pressure vessel steel. Three regions of behavior are indicated: (a) slow growth near the threshold ΔK_{th}, (b) intermediate region following a power equation, and (c) unstable rapid growth. (Plotted from the original data for the study of [Paris 72].)

From Mechanical Behavior of Materials, Norman E. Dowling

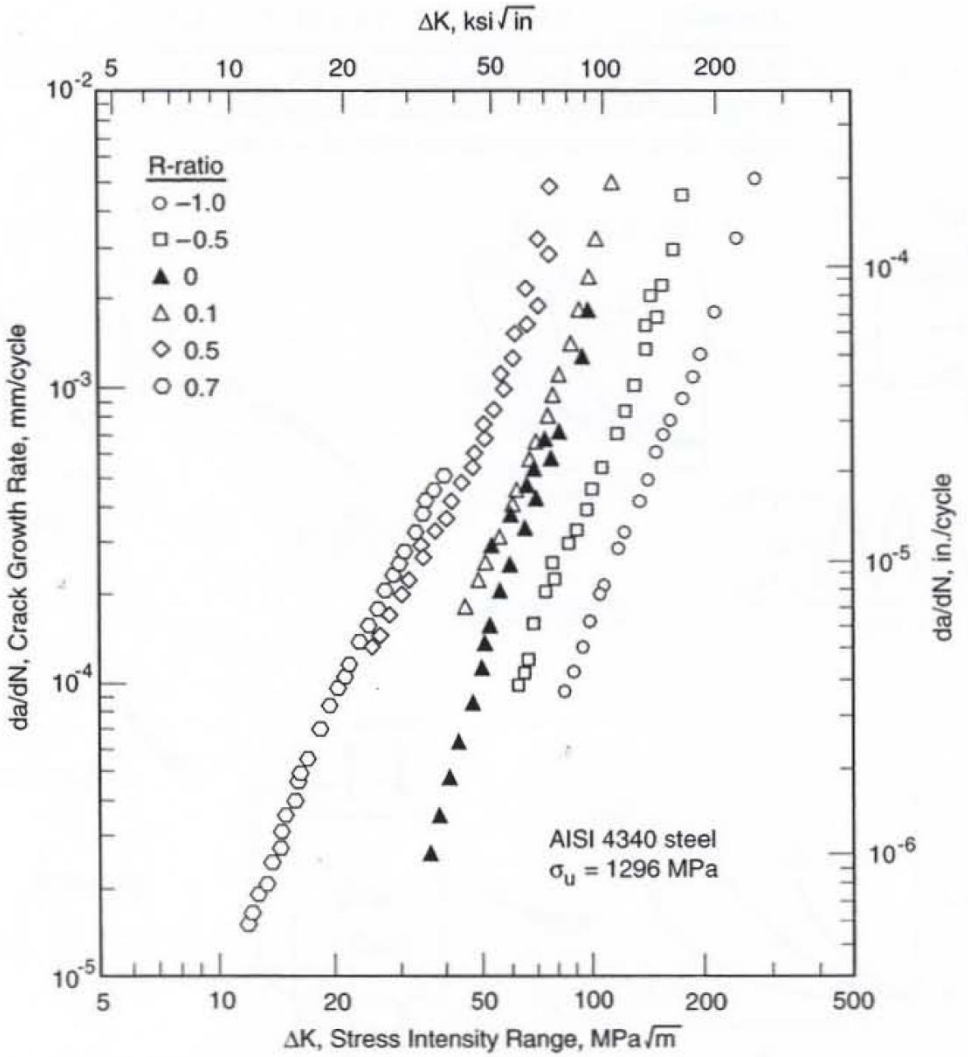

Figure 11.4 Effect of R-ratio on crack growth rates for an alloy steel. For $R < 0$, the compressive portion of the load cycle is here included in calculating ΔK. (Data from [Dennis 86].)

From Mechanical Behavior of Materials, Norman E. Dowling

Example 14.3

Consider long crack propagation under fatigue. Develop an expression for the number of cycles, ΔN, required for a crack to grow from an initial length a_i to a final length a_f, Given that $\Delta K = Y\Delta\sigma\sqrt{\pi a}$ and $da/dN = C\Delta K^m$, where the symbols have their usual significance. Discuss the implications of the expression.

Solution:

$$
\begin{aligned}
da/dN &= C\,\Delta K^{\,m}, \\
\Delta N &= \int_{a_i}^{a_f} \frac{da}{C\,\Delta K^{\,m}} \\
&= \int_{a_i}^{a_f} \frac{da}{C\,(Y\,\Delta\sigma\sqrt{\pi})^m a^{m/2}} \\
&= \frac{a_f^{(1-m/2)} - a_i^{(1-m/2)}}{C\,(Y\,\Delta\sigma\sqrt{\pi})^m (1-m/2)} \\
&= \frac{1-(a_i/a_f)^{m/2-1}}{C\,(Y\,\Delta\sigma\sqrt{\pi})^m (m/2-1)} \left(\frac{1}{a_f^{m/2}-1}\right).
\end{aligned}
$$

The implications of the expression are that it is not valid for $m = 2$ and that ΔN is more sensitive to the initial crack length a_i than the final crack length a_f.

Example 14.4

The fatigue crack markings shown in Figure E14.4 were found in a fractured part. Determine the time to rupture of this part if the loading frequency is 10 Hz, the maximum stress applied to the part is 300 MPa, and the minimum stress is zero. The initiation stage of the flaw is 50% of the life of the part.

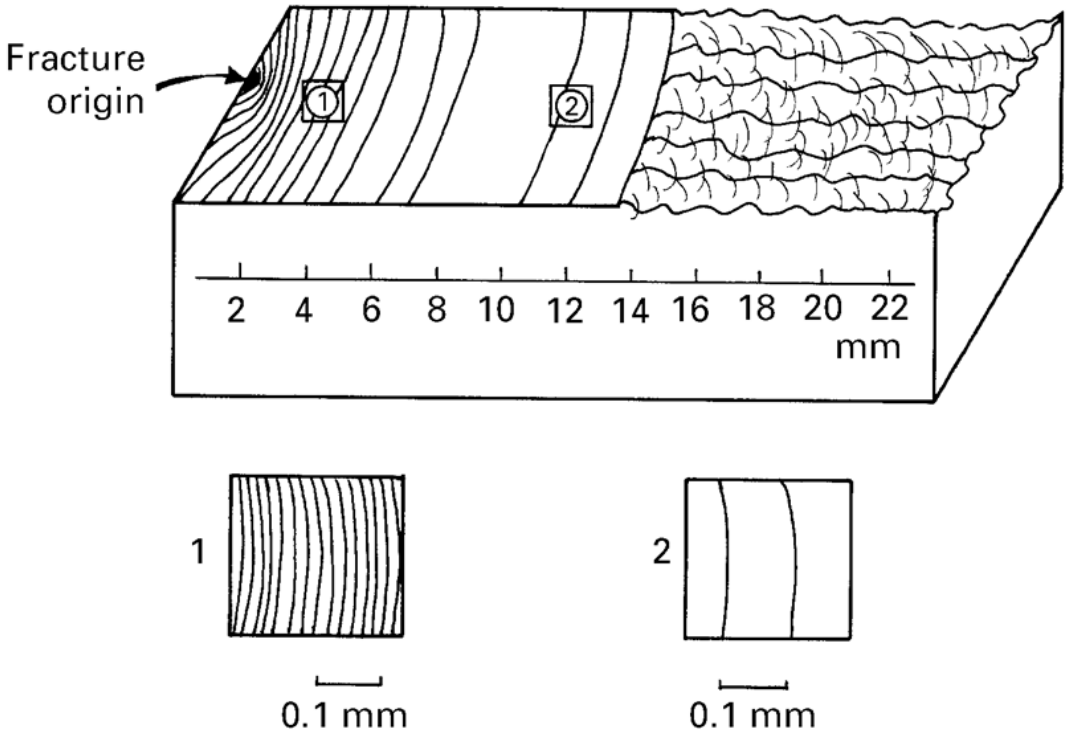

Solution: We have

$$\left(\frac{da}{dN}\right)_1 = 0.016 \text{ mm}, \left(\frac{da}{dN}\right)_2 = 0.1 \text{ mm},$$
$$a_1 = 2 \text{ mm}, a_2 = 10 \text{ mm}.$$

Fracture occurs when $a_f = 14$ mm. Assuming that we have plane strain,

$$\begin{aligned} K_{Ic} &= 1.12\sigma\sqrt{\pi a} \\ &= 1.12 \times 300\sqrt{\pi \times 0.014} \\ &= 70 \text{ MPa m}^{1/2}. \end{aligned}$$

We now find the parameters for the Paris equation:

$$\begin{aligned} \frac{da}{dN} &= C(\Delta K)^m, \\ \Delta K_1 &= 1.12\sigma\sqrt{\pi a_1} = 1.12 \times 300\sqrt{\pi \times 2 \times 10^{-3}} \\ &= 26.6 \text{ MPa m}^{1/2}, \\ \Delta K_2 &= 1.12\sigma\sqrt{\pi a_2} = 1.12 \times 300\sqrt{\pi \times 10 \times 10^{-3}} \\ &= 59.55 \text{ MPa m}^{1/2}, \\ 0.016 \times 10^{-3} &= C(26.6)^m, \\ 0.1 \times 10^{-3} &= C(59.55)^m, \\ m &= 2.27, \\ C &= 0.94 \times 10^{-8}, \end{aligned}$$

$$\frac{da}{dN} = 0.94 \times 10^{-8}(\Delta K)^m = 0.94 \times 10^{-8} \times (1.12 \times 300\sqrt{\pi a})^{2.27},$$

$$\frac{da}{a^{1.135}} = 0.019\, dN.$$

Integrating between the limits, $a_f = 14$ mm and $a_i = 0.02$ mm, we get:

$$\int_{a_i}^{a_f} \frac{da}{a^{1.135}} = \int_{0.02}^{14} \frac{da}{a^{1.135}} = 0.019 \int dN = 0.019N,$$

$$a_0 = 0.02\,\text{mm}$$

$$a_f = 14\,\text{mm}$$

$$0.019N = \frac{-1}{0.135 \times (14 \times 10^{-3})^{0.135}} + \frac{1}{0.135 \times (0.02 \times 10^{-3})^{0.135}}$$

Each cycle corresponds to 0.1 s, so

$$t = 0.1N$$

The total time is equal to the initiation time plus the propagation time:

$$t = 2t = 98.6 \times 2\,\text{s}$$

$$= 197.2\,\text{s}.$$